4-1-1997

ATLSS Precast Concrete Systems: Design Examples and Seismic Analysis

Janekrisana Kanatharana

Le-Wu Lu

B. Vincent Viscomi

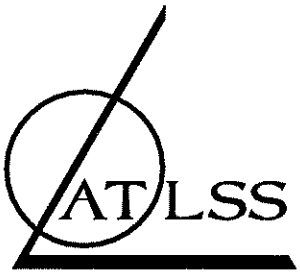

ADVANCED TECHNOLOGY FOR
LARGE
STRUCTURAL SYSTEMS

Lehigh University

ATLSS Precast Concrete Systems:

Design Examples and Seismic Analysis

by

Janekrisana Kanatharana

Le-Wu Lu

B. Vincent Viscomi

ATLSS Report No. 97-03

April 1997

An NSF Sponsored Engineering Research Center

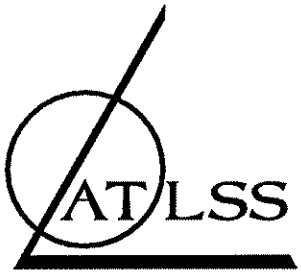

ADVANCED TECHNOLOGY FOR
LARGE
STRUCTURAL SYSTEMS

Lehigh University

ATLSS Precast Concrete Systems:

Design Examples and Seismic Analysis

by

Janekrisana Kanatharana
Former Graduate Research Assistant

Le-Wu Lu
Chairman, Civil and Environmental Engineering

B. Vincent Viscomi
Research Professor

ATLSS Report No. 97-03

April 1997

ATLSS Engineering Research Center
Lehigh University
117 ATLSS Dr., Imbt Laboratories
Bethlehem, PA 18015-4729
(610) 758-3525

An NSF Sponsored Engineering Research Center

ABSTRACT

This report concludes a series of three reports based on research studies on ATLSS Precast Concrete (APC) systems, conducted at the Center for Advanced Technology for Large Structural Systems (ATLSS) at Lehigh University. The APC systems are primarily for, but not limited to, low- to mid-rise buildings in moderate seismic zones. There are two APC designs: a Modified ATLSS Passage Type design (MAPT) and an ATLSS Nodal Type (ANT) design.

The current report presents design methodologies for seismic-resistant beams, columns, and beam-column connections of APC systems, describes seismic analyses of structures with APC systems, and gives design examples for both MAPT and ANT systems.

Conclusions from this latest study are that APC systems can be designed to satisfy strong column-weak beam behavior, which is the current design philosophy for seismic-resistant structures. Moreover, based on both static inelastic and dynamic inelastic analyses (the latter using both Nahanni and El Centro earthquake records), APC systems could be designed and qualified for use in severe seismic zones such as UBC zone 4.

ACKNOWLEDGEMENTS

This research was funded by the Center for Advanced Technology for Large Structural Systems (ATLSS) at Lehigh University, as part of ATLSS project ADC-03: ATLSS Connections and Structural Systems. The ATLSS Center is an Engineering Research Center supported in part by a grant from the National Science Foundation (NSF). Dr. John W. Fisher is the Director of ATLSS.

The authors acknowledge the assistance provided by the Technical Activities Council of the Precast/Prestressed Concrete Institute (PCI) and its industry partners. Appreciation is also extended to Splice Sleeve of North America, Inc. (Mr. Alvin C. Ericson, Technical Consultant) and Master Builders, Inc. for donating materials used in the earlier experimental portion of this research.

Opinions, findings, and conclusions expressed in this report are solely those of the authors, and do not necessarily reflect the views of the sponsors or those acknowledged above.

1. INTRODUCTION

ATLSS has conducted a study in which new precast concrete beam-to-column connections, called ATLSS Precast Concrete (APC) systems, were conceptually developed and large-size prototypes were designed, fabricated, and tested to examine their behavior under constant column load, but increasing cyclic beam loadings. An emphasis with the APC systems has been their suitability as seismic-resistant systems and, consequently, the study included a review of design methodologies for concrete seismic-resistant structures.

In the initial report [1] of the study, a state-of-the-practice review was made of existing precast concrete connections, and a conceptual development of new two-dimensional ATLSS precast concrete beam-to-column and beam-to-beam connections was described. Two types of APC systems were conceived; MAPT (modified ATLSS passage type) and ANT (ATLSS nodal type). In the second report [2] of the overall study, the emphasis was on design methodology and performance evaluation. A review of current design methodologies for concrete seismic-resistant structures was presented and, for a prototype structure, designs for the MAPT and ANT connections were developed and served as the basis for an experimental evaluation program. Six large-scale, but half-size, test systems, three type MAPT and three type ANT, were fabricated for the execution of the test program. The critical experimental observations and the capacities of the connection systems were described.

In this third report, design methodologies are presented for seismic-resistant beams, columns, and beam-column connections of APC systems, using findings from the earlier reports; seismic analyses of structures with APC systems are described; and design examples for both MAPT and ANT systems are given.

2. DESIGN METHODOLOGIES AND EXAMPLES FOR APC CONNECTION SYSTEMS

2.1 Design Objectives

The philosophy and current practices of earthquake-resistant design are that, to withstand seismic excitations, structures in general should be designed for strong column-weak beam behavior, which enables the designer to better control the behavior of the structures. Experimental work reported previously [2] on precast beam-column subassembly specimens of the APC systems has shown that with proper design and detailing, it is possible to develop hinging at the desired locations and thus improve the seismic response characteristics of a given structure. Therefore, design methodologies for beams, columns, and beam-column connections of APC systems are proposed herein

Although this study was carried out for a prototype structure located in a zone of moderate seismicity, the proposed design methodologies should be are applicable to APC systems constructed in all seismic zones. The reason for this is that the proposed design methodologies are "strength-based" and are independent of the specific seismic zones. Moreover, the ductility capacities of the APC systems can be ensured by applying the appropriate transverse reinforcement details at the plastic hinge locations.

These details for structures in various seismic zones are given in the provisions of the ACI 318-89 code [3], which is incorporated as a part of the proposed design methodologies.

To illustrate the application of the proposed design methods, design examples for beams, columns, and connections are also presented.

The design objective for APC systems for seismic resistance is to achieve strong column-weak beam behavior via formation of plastic hinges in the beams, not in the beam-column connections or in the columns except at the base of the first story columns. This objective can be achieved by developing a desired sequence of plastification in the structure through careful design and selection of its members. By requiring hinges to form in the beams away from the connections, excessive inelastic deformations are prevented from spreading into the connections, where they result in rapid loss of connection strength and stiffness and also lead to reduction of ductility and energy dissipation capacities. Instead, when excessive inelastic deformations occur exclusively in the beams, it is possible to achieve only gradual strength degradation and large ductility and energy dissipation.

Structures designed for earthquake zones should also have a distinct restricted yielding range prior to an unrestricted yielding range. The distinct restricted yielding range can be obtained by selecting members with good inelastic deformation capabilities to yield first, thus dissipating much of the input seismic energy. Members with less inelastic capacities are designed to yield later. In structures with distinct restricted yielding, elastic restoring forces tend to reduce the drift of the structures and also cause it to vibrate about a mean position, rather than accumulate progressive lateral drifts leading to possible overall collapse.

2.2 Beam and Column Design Methodology

Beams and columns for APC systems should be designed and detailed using the appropriate provisions of the ACI 318-89 code [3] or its later revisions. The beam design should precede the column design. In the beam design, the beam sections at the designated hinging locations (DHLs) are the sections with the lowest strength-to-design moment ratios. This ratio is defined as the moment capacity of the section computed using ACI 318-89, divided by the factored design moment of the section. The factored design moment is obtained from structural analysis.

DHLs should be located away from the column faces at a distance equal to the larger of (1) one beam depth, as suggested by Wight, et al. [4 and 5], or (2) the tensile development length of the largest beam longitudinal reinforcement to be used at the column faces (CFs) and to be terminated at the DHLs. The distance of one beam depth away from the CFs prevents excessive inelastic deformation from spreading into the connections; the distance of one tensile development length ensures that the full beam moment capacity develops at the CFs. Because larger reinforcement has a larger tensile development length, and because rotational ductility demands increase when plastic hinges are to form further away from the connections, the smallest *practical* beam longitudinal reinforcement should be used to keep DHLs as close as possible to the CFs (but not closer than one beam depth).

The moment strength of the beam sections at the CFs should be no less than the upgraded design moment produced by the upgraded applied loads at failure. The upgraded applied loads at failure are proportional to the factored design loads, and result in plastic hinge formations at the DHLs, assuming that the yield strength of the beam longitudinal reinforcement at the DHLs is 1.25 times the nominal yield strength. The use of the upgraded design moment ensures that the CF sections will not experience excessive yielding when strain hardening occurs at the DHL sections.

After the beams have been designed, the columns are designed for their load effects. The first is that produced by the factored design axial forces and moments from the governing gravity load combination. The second is that originating from the more critical of (1) the factored design axial forces and moments from the governing lateral load combination, or (2) the factored design axial forces from the governing lateral load combinations and the column moments corresponding to the upgraded applied loads at failure. The resulting column moments from the upgraded applied loads at failure are the theoretically largest moments that the columns can experience near the connections when the failure mechanism of the structure occurs.

2.3 Connection Design Methodology

The proposed design methodology for APC connections is based on a strut-and-tie model, referred to hereafter as the unified two-dimensional strut-and-tie model for APC connections. The unified strut-and-tie model is essentially the two-dimensional strut-and-tie model utilized in designing the connections included in the earlier experimental study (Group B ANT specimens)[2].

The assumptions stipulated for the unified strut-and-tie model are as follows:

1. The centroids of the beam horizontal struts and ties coincide with the centroids of the compressive stress block and the tensile reinforcement of the CF sections, respectively.
2. The centroids of the column vertical struts and ties lie in the same planes as the centroids of the compressive stress block and the tensile reinforcement of the column sections adjacent to the connection.

For the second assumption, the centroid of the compressive stress block can be calculated using the factored axial force of the governing lateral load combination, divided by the appropriate column strength reduction factor, and the moment strength of the section under the axial force.

Two unified strut-and-tie models are required due to the reversal of the lateral loading. The models for each connection should be constructed to include the entire connection and portions of the beams and columns bounded by their points of contraflexure. For column portions, the column mid-heights may be used in lieu of the actual points of contraflexure (except for the columns in the bottom story). When the connections being designed represent a group of connections, the average locations of the points of contraflexure may be used. At the points of contraflexure, only the beam shear forces and their equilibrating column reaction forces are applied to the strut-and-tie models. This is because the column axial force does not cause fanning inside the connection; thus it is not required in proportioning the connection reinforcement. The magnitude of the beam shear forces should be equal to the upgraded design moments of the beam CF sections, divided by the distances from the CF sections to the points of contraflexure. This practice maintains the *correct* magnitudes of moments acting at the connections at all times, even when the points of contraflexure are shifted from their actual locations.

Reinforcement inside and around the connection should be proportioned to withstand the splitting tensile forces induced by fanning of the diagonal compressive struts and the vertical compressive struts. The diagonal compressive struts are located inside the connection, while the vertical compressive struts are immediately above and below the connection. The magnitude of the splitting tensile forces are computed using a fanning slope of 2, as suggested by Schlaich, et al. [6].

Horizontal, vertical and diagonal reinforcement are used inside the connection to resist the splitting tensile forces caused by fanning, whereas only horizontal reinforcement is used in the columns

above and below the connection for constructablility. Eqs. (3-7), (3-2), (3-3), (3-14), and (3-15) in Ref.[2] should be used sequentially in proportioning the reinforcement inside the connection, and Eqs. (3-2), (3-3) and (3-6) for the reinforcement above and below. For exterior or corner connections, diagonal reinforcement should not be considered active in reducing fanning of the diagonal compressive struts, due to its inadequate anchorage space in compression. Thus, the area of the diagonal rebar pair in Eq. (3-7) should be considered as zero when designing for the exterior and corner connections. In arranging reinforcement inside APC connections, the diagonal reinforcement and, if possible, some of the horizontal reinforcement are extended to the DHL sections. Due to its position, the contribution of the extended portion of the diagonal reinforcement can be included in computing the moment strengths of the CF sections, whereas that of the horizontal reinforcement should be excluded. Connection reinforcement that is not extended to the DHL sections must be looped.

In the special case of MAPT connections, most reinforcement against the splitting tensile forces of the diagonal struts should be placed inside the captive beam portion, and each column web should be designed as an individual column subjected to one-half the factored design axial force of the governing lateral load combination. Design attention should be focused on column web stability. These recommendations result from experimental observations that, in the descending stages, the captive beam portion of MAPT connections carries most of the beam moment and the column webs withstand practically all the axial force.

2.4 Design Examples

Design examples are presented for beams, columns and beam-column connections of both MAPT and ANT APC systems, using the proposed design methodologies. Figure 2-1 shows part of a frame containing the beams, the columns and the beam-column connections to be designed. The frame is located in a moderate seismic zone, and the design for lateral load resistance is governed by the earthquake load combinations. The factored design loads of the beams and the columns are summarized in Table 2-1, and the governing design bending moment diagrams are shown in Figs. 2-2 and 2-3, respectively. The factored design loads of the connections are not included in Table 2-1, because they must be calculated after the beams have been designed.

Table 2-1 Factored Design Loads for Beams and Columns of MAPT and ANT Assemblies

Member Group* (1)	Load Case (2)	Axial (kip) (3)	$M_{left/bottom}$* (kip-in) (4)	$M_{right/top}$ (kip-in) (5)	$V_{left/bottom}$* (kip) (6)	$V_{right/top}$ (kip) (7)	w_{DU}* (kip/in) (8)
B1	Gravity	-	-190.79	-165.31	3.76	-3.56	24.50×10^{-3}
	Earthquake	-	-1961.38	1703.20	14.58	9.85	15.75×10^{-3}
B2	Gravity	-	-184.18	-183.49	3.68	-3.67	24.50×10^{-3}
	Earthquake	-	1702.84	-1937.75	-9.77	-14.50	15.75×10^{-3}
C1	Gravity	845.98	-41.70	-77.28	0.99	-0.99	-
	Earthquake	701.13	-2029.10	361.44	19.92	19.92	-
C2	Gravity	1133.20	-	-	-	-	-
	Earthquake	849.87	-3203.41	739.92	32.86	32.86	-

* See Fig. 2-1 for locations of members, and Figs. 2-2 and 2-3 for sign conventions.

Concrete with a nominal strength of 4000 psi and elastic modulus of 3605 ksi is assumed for the MAPT assemblies; in contrast, a nominal strength and an elastic modulus of 6000 psi and 4415 ksi are used for the ANT assemblies. The steel reinforcement has a nominal yield strength of 60 ksi and an elastic modulus of 29,000 ksi .

2.4.1 Design of Beams and Columns for MAPT Assemblies

A) Beam B1

- **Initial Parameters**

assumed beam dimensions	= 10 x 25	in.
assumed column depth	= 16	in.
largest reinforcement size (bundled in groups of 2)	= DB6	
estimated tensile development length	= 21	in.
dist. from column faces to DHLs	= 25	in.
factored design moment at left DHL section	= 1488.88	kip-in.
factored design moment at right DHL section	= 1369.55	kip-in.
factored design moment at left CF section	= 1845.26	kip-in.
factored design moment at right CF section	= 1623.94	kip-in.

- **Left and Right DHL Sections**

Try:

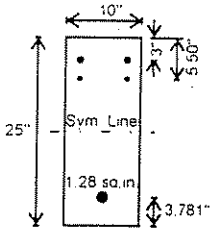

$f'_c = 4000$ psi., $f_Y = 60$ ksi.

$E_c = 3605$ ksi., $E_s = 29000$ ksi.

$\beta_1 = 0.85$

$\rho = \rho' = A_s/bd = 6.0 \times 10^{-3} \geq \rho_{min} = 3.3 \times 10^{-3}$

$\rho < 0.75\rho_b = 21.4 \times 10^{-3}$ ok.

Assume tensile steel yields and compressive steel does not; then,

$$\varepsilon_s' = 0.003\ (c - 3.781) / c = 0.003 - 11.343 \times 10^{-3} / c$$

$$\varepsilon_s = 0.003\ (21.219 - c) / c = 63.657 \times 10^{-3} / c - 0.003$$

$$C_1 = 0.85\ f'_c\ b\ \beta_1 c = 0.85 \times 4 \times 10 \times 0.85c = 28.90c$$

$$C_2 = A_s'\ E_s\ \varepsilon_s' = 111.36 - 421.05 / c$$

$$T = A_s\ f_Y = 1.28 \times 60 = 76.80 \text{ kips}$$

Solve: $c = 3.27$ in., $\varepsilon_s' = -0.474 \times 10^{-3}$, $\varepsilon_s = 16.492 \times 10^{-3} > \varepsilon_Y$ ok.

$C_1 = 94.38$ kips, $C_2 = -17.58$ kips (tension), $T = 76.80$ kips

$M_n = 1565.08$ kip-in., $\phi_b M_n = 1408.57$ kip-in. $\approx M_u$ ok.

To account for the potential strain hardening, assume $f_Y = 1.25 \times 60 = 75$ ksi.

Solve: $c = 3.56$ in., $\varepsilon_s' = -0.186 \times 10^{-3}$, $\varepsilon_s = 14.879 \times 10^{-3} > \varepsilon_Y$

$C_1 = 102.90$ kips, $C_2 = -6.90$ kips (tension), $T = 96.00$ kips
$M_n = 1907.40$ kip-in.

At left DHL section, overstrength factor due to strain hardening (O_ε) =

$M_n/M_u = 1907.40 / 1488.88 = 1.281$

At right DHL section, $O_\varepsilon = 1907.40 / 1369.55 = 1.393$

- **Left and Right CF Sections**

Try:

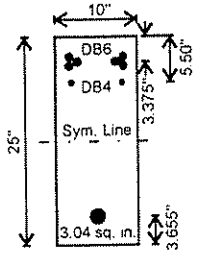

$f'_c = 4000$ psi., $f_Y = 60$ ksi.

$E_c = 3605$ ksi., $E_s = 29000$ ksi.

$\beta_1 = 0.85$

$\rho = \rho' = A_s/bd = 14.24 \times 10^{-3} \geq \rho_{min} = 3.3 \times 10^{-3}$

$\rho < 0.75\rho_b = 21.4 \times 10^{-3}$ ok.

Assume tensile steel yields and compressive steel does not; then,

$\varepsilon_s' = 0.003\ (c - 3.655) / c = 0.003 - 10.965 \times 10^{-3} / c$

$\varepsilon_s = 0.003\ (21.345 - c) / c = 64.04 \times 10^{-3} / c - 0.003$

$C_1 = 0.85\ f'_c\ b\ \beta_1 c = 0.85 \times 4 \times 10 \times 0.85c = 28.90c$

$C_2 = A_s'\ E_s\ \varepsilon_s' = 264.48 - 966.674 / c$

$T = A_s\ f_Y = 3.04 \times 60 = 182.40$ kips

Solve: $c = 4.54$ in., $\varepsilon_s' = 0.582 \times 10^{-3}$, $\varepsilon_s = 11.119 \times 10^{-3} > \varepsilon_Y$ ok.

$C_1 = 131.07$ kips, $C_2 = 51.33$ kips, $T = 182.40$ kips

$M_n = 3453.08$ kip-in., $\phi_b M_n = 3107.77$ kip-in

To ensure that the plastic hinges will not form at the CF sections, the moment strength of the CF sections must be larger than the "upgraded" design moments.

At left CF section, $\phi_b M_n > O_\varepsilon M_u = 1.281 \times 1845.26 = 2363.78$ kip-in. ok.
At right CF section, $\phi_b M_n > O_\varepsilon M_u = 1.392 \times 1623.94 = 2261.69$ kip-in. ok.

- **Shear Reinforcement**

1) Within Two Beam Depths from Column Faces (Section 21.9 ACI 318-89)

$V_u = 2M_{n\ @\ CF} / L_n$; L_n = clear span length = span length - column width

$= 2 \times 2545.60 / (300 - 16) = 17.93$ kips

or $V_u = V_{u,2E} \approx 2V_{u,\ governing\ EQ\ Load\ case}$

$= 2 \times 14.58 = 29.16$ kips ← governs

$V_c = 2 (f'_c)^{1/2} bd / 1000 = 2 (4000)^{1/2} \times 10 \times (25 - 3.463) / 1000 = 27.24$ kips

use DB4 stirrups @ max. allow. Spacing (S_{max})

S_{max} = min (0.25d = 5.38", $8d_b = 8 \times 6/8 = 6$", 24 x dia. Stirrups = 12", 12") ≈ 5 in.

$\therefore V_s = A_v f_Y d / S_{max} = 0.40 \times 60 \times 21.537 / 5 = 103.38$ kips

$\phi V_n = \phi(V_c + V_s) >> V_u$ ok. → use DB4 stirrups @ 5 in. spacing.

2) Outside Two Beam Depths from Column Faces (Section 11.5 ACI 318-89)

$V_u = 14.58$ kips

The sections have enough shear capacity because $V_c = 27.24$ kips (from above).

$\therefore$ use DB4 stirrups @ max. allow. spacing (S_{max}) = 0.50d = 10.76 ≈ 10 in.

B) Beam B2

The design loads of beams B1 and B2 are roughly identical; therefore, identical designs are used for Beams B1 and B2.

C) Column C1

- **Initial Parameters**

assumed column dimensions	= 16 x 24	in.
largest reinforcement size	= DB8	

- **All Column Sections**

Try:

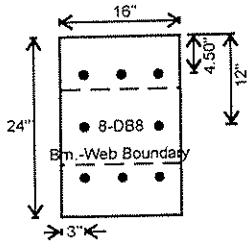

$f'_c = 4000$ psi., $f_Y = 60$ ksi.

$E_c = 3605$ ksi., $E_s = 29000$ ksi.

$\beta_1 = 0.85$, $\phi_c = 0.70$, $\phi_b = 0.90$

$A_s = 6.32$ in.^{2}, $A_g = 384$ in.^{2} → $A_s/A_g = 0.0165 > 0.01$ ok.

Gravity Load Case: $P_u = 845.98$ kips, $M_u \approx 0$ kip-in.

EQ. Load Case: $P_u = 701.13$ kips, and

$M_u = 2029.12$ kip-in. ← governs

or $P_u = 701.13$ kips, and

$M_u = (0.50\ O_E M_u)$@ left end of beam B1

$= 0.50 \times 1.281 \times 1961.3 = \underline{1256.26 \text{ kip-in.}}$

From the interaction curve (Fig. 2-4a), this assumed section is adequate.

$\therefore$ use this assumed section for column C1.

- **Shear Reinforcement**

1) Within the Length L_o from Joint Faces (Section 21.9 ACI 318-89)

$L_o = \max(H_n/6, b_c, h_c)$;

H_n = clear column height = 120 - 25 = 95 in.; $H_n/6 = 24$ in.;

b_c = column width = 24 in.;
h_c = column depth = 16 in.

$V_u = 2M_{n\ @\ joint\ face} / h_n$; use $M_n = M_{n,balance} = 3822.86$ kip-in.

$= 2 \times 3822.86 / 95 = 80.48$ kips $\leftarrow$ governs

or $V_u = V_{u,2E} \approx (2V_u)$ governing EQ Load case

$= 2 \times 19.92 = 39.84$ kips

$V_c = 2 (f'_c)^{1/2} b_c d_c / 1000 = 2 (4000)^{1/2} \times 24 \times (16 - 3) / 1000 = 39.47$ kips

use DB4 ties + one DB4 cross-tie per tie @ max. allowable spacing S_{max}:

S_{max} = min ($8d_b = 8 \times 1 = 8$", 24 x dia. stirrups = 12", $0.50h_c = 8$", 12") = 8 in.

$\therefore V_s = A_v f_Y d / S_{max} = 0.60 \times 60 \times (16-3) / 8 = 58.50$ kips

$\phi V_n = \phi(V_c + V_s) = 0.85(39.47+58.50) = 83.27$ kips $> V_u$ ok.

$\therefore$ Use DB4 ties with one DB4 cross-tie per tie @ 8" spacing.

2) Outside the Length L_o (Section 11.5 ACI 318-89)

$V_u = 19.92$ kips

The sections have enough shear capacity; therefore, after the distance of 24" from joint faces, use DB4 ties with one DB4 cross-tie

@ max. allowable spacing (S_{max}) = $0.50h_c = 8$ in.

D) Column C2

- **Initial Parameters**

assumed column dimensions	= 18 x 24	in.
largest reinforcement size	= DB10	

- **All Column Sections**

Try:

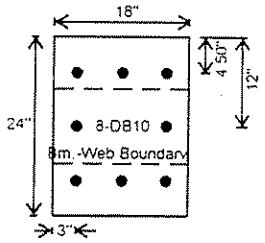

$f'_c = 4000$ psi., $f_Y = 60$ ksi.

$E_c = 3605$ ksi., $E_s = 29000$ ksi.

$\beta_1 = 0.85$, $\phi_c = 0.70$, $\phi_b = 0.90$

$A_s = 10.16$ in.^{2}, $A_g = 432$ in.^{2} $\rightarrow$ $A_s/A_g = 0.0235 > 0.01$ ok.

Gravity Load Case: $P_u = 1133.20$ kips, $M_u \approx 0$ kip-in.

EQ. Load Case: $P_u = 849.87$ kips, and

$M_u = 3203.41$ kip-in. $\leftarrow$ governs

or $P_u = 849.87$ kips, and

$M_u = (0.50\ O_E M_u)_{\text{approx. @ left end of beam B1}}$

$= 0.50 \times 1.281 \times 1961.3 = 1256.26$ kip-in.

From the interaction curve (Fig. 2-4b), this assumed section is adequate.

$\therefore$ use this assumed section for column C2.

- **Shear Reinforcement**

1) Within the Length L_o from Joint Faces (Section 21.9 ACI 318-89)

$L_o = \max(H_n/6, b_c, h_c)$;

H_n = clear column height = 120 - 25 = 95 in.; $H_n/6 = 15.8$ in.

b_c = column width = 24 in.,
h_c = column depth = 18 in.

$V_u = 2M_{n\ @\ \text{joint face}} / h_n$; use $M_n = M_{n,\text{balance}} = 4080$ kip-in.

$= 2 \times 4080 / 95 = 85.89$ kips $\leftarrow$ governs

or $V_u = V_{u,2E} \approx (2V_u)_{\text{governing EQ Load case}}$

$= 2 \times 32.85 = 65.70$ kips

$V_c = 2 (f'_c)^{1/2} b_c d_c / 1000 = 2 (4000)^{1/2} \times 24 \times (18 - 3) / 1000 = 45.54$ kips

Use DB4 ties and one DB4 cross-tie per tie @ max. allowable spacing (S_{max})

$S_{max} = \min(8d_b = 8 \times 1 = 8", 24 \times \text{dia. Stirrups} = 12", 0.50h_c = 9", 12") = 8$ in.

$\therefore V_s = A_v f_Y d/S_{max} = 0.60 \times 60 \times (16-3) / 8 = 58.50$ kips

$\phi V_n = \phi(V_c+V_s) = 0.85(45.54+58.50) = 88.43$ kips $> V_u$ ok.

$\therefore$ use DB4 ties with one DB4 cross-tie per tie @ 8" spacing.

2) Outside the Length L_0 (Section 11.5 ACI 318-89)

$V_u = 32.86$ kips

The sections have enough shear capacity, therefore, after the distance of 24" from joint faces, use DB4 ties w/ one DB4 cross-tie

@ approx. max. allow. spacing (S_{max}) = $0.50h_c = 9$ in. ≈ 8 in.

2.4.2 Design of Regular MAPT Connections

Figure 2-5 depicts the strut-and-tie model for the regular connections shown in Fig. 2-1. Because the connections represent a group of beam-column connections, the average locations of points of contraflexure are used for the beam portions of the strut-and-tie model. In addition, the points of contraflexure for the column portions are assumed at the column mid-heights, and the centroids of the struts and ties forces are according to the assumptions stipulated in Section 2.3. The applied shear forces at the ends of the beam portions assumed equal to the larger upgraded design moments at the beam CF sections, divided by the distances from the CF sections to the end of the beam portions.

• **Captive Beam Portion**

$C_d = 480.51$ kips, from Fig. 2-5.

Try reinforcing the diagonal compressive strut with one pair of DB6 diagonal rebars at a 60° inclination angle measured from horizontal axis.

Apply Eq. (3-7) from [2]:

$C_f = 480.51 - 0.85 \times (2 \times 0.44) \times 60 \times \cos(\theta_3 - 60)$;

$\theta_3 = 72.97°$, see Fig.2-5.

$\therefore C_f = 480.51 - 43.74 = 436.77$ kips

Compute T_n:

$T_n = C_f / 4\phi_D$, Eq. (3-2) from [2].

$\therefore T_n = 436.77 / (4 \times 0.85) = 128.46$ kips

Calculate A_S:

$A_s = kT_n / f_Y$ and $k = 2$ for diagonal compressive struts.

$\therefore A_s = 2 \times 128.46 / 60 = 4.28$ in^2.

Reinforce the splitting tensile forces with another pair of diagonal rebars crossing the first pair, and compute the amount of horizontal and vertical reinforcement, using Eqs. (3-14) and (3-15) from [2]:

$A_{sh} = (4.28 - (2 \times 0.44) \times \cos(90 + \alpha - 2\theta_3)) \sin(\theta_3)$;

$\alpha = \theta_3 - 60.$

$\therefore A_{sh} = (4.28 - 0.64) \sin(\theta_3) = 3.48 \text{ in}^2.$

Similarly,

$\therefore A_{sv} = (4.28 - 0.64) \cos(\theta_3) = 1.07 \text{ in}^2.$

→ Use 6 DB4 horizontal stirrups and 3 pairs of DB4 intermediate long. rebar layers. This provides:

$A_{sh} = 3.60 \text{ in}^2.$

→ Use 3 DB4 vertical stirrups within the center portion. This provides:

$A_{sv} = 1.20 \text{ in}^2.$

- **<u>Reinforcement for Column Portions Immediately Above and Below the Beam</u>**

$C_f = C_d = 175.49$ kips, from Fig. 2-5.

Compute T_n:

$T_n = C_f / 4\phi_D$, Eq. (3-2) from [2]

$\therefore T_n = 175.49 / (4 \times 0.85) = 51.61$ kips

Calculate A_S:

$A_s = kT_n / f_Y$,and k = 1 for vertical compressive struts.

$\therefore A_s = A_{sh} = 1 \times 51.61 / 60 = 0.86 \text{ in}^2.$

→ Use 2 DB4 horizontal stirrups within 10" distance above and below the captive beam portion; 10" being approximately the length of the vertical compressive struts, Fig. 2-5.

$\therefore A_{sh} = 0.80 \text{ in}^2.$

- **<u>Column Webs</u>**

From Section 10.3 of ACI 318-89,

$P_{u,max}$ of column $= 0.80\phi_c [0.85f'_c (A_g - A_{st}) + f_Y A_{st}]$

where $P_{u,max}$ = maximum allowable factored design axial load,
A_g = gross sectional area of column, and
A_{st} = total longitudinal steel area in the column section.

For each column web,

$P_u = 0.50 \times 849.87 = 424.94$ kips

$A_g = 7 \times 18 = 126$ in^2.

$A_{st} = 3 \times$ Area of DB10 $= 3 \times 1.27 = 3.81$ in^2.

$\therefore P_{u,max} = 0.80 \times 0.70 \times [0.85 \times 4000/1000 \times (126 - 3.81) + 60 \times 3.81]$

$= 360.67$ kips $< P_u$ Nok.

Add 3-DB6 along the outer perimeter of each web,

$\rightarrow A_{st} = 3 \times 1.27 + 3 \times 0.44 = 5.13$ in^2.

$\therefore P_{u,max} = 0.80 \times 0.70 \times [0.85 \times 4000/1000 \times (126 - 5.13) + 60 \times 5.13]$

$= 402.50$ kips $\approx P_u$ ok.

Had the original reinforcement inside the column web been adequate, at least two additional rebars would have had to be added to the column web at the corners of the outer parameter, to conform with the requirements of Section 10.9 of ACI 318-89 .

- **Stability of Column Webs**

The commentary of Section 10.10 of ACI 318-89 provides an equation for approximating the flexural rigidity (EI) of a column when examining the column stability:

$EI = E_c I_g (0.20 + \rho_t E_s / E_c)$

where E_c = Elastic Modulus of Concrete = 3605 ksi

E_s = Elastic Modulus of Steel = 29000 ksi.

I_g = gross moment of inertia about weak-axis = $1/12 \times 18 \times 6.5^3 = 411.94$ in^4.

ρ_t = reinforcement ratio = $A_{st} / bd = 5.13 / (6.5 \times 15) = 0.053$

$\therefore EI = 3605 \times 411.94 \times (0.20 + 0.053 \times 29000 / 3605) = 930.16 \times 10^3$ kip-in^2.

Assume the column webs are fully braced and have fixed-fixed end condition.

$P_{cr} = \pi^2 EI / L^2$; L = one-half the length of column webs = 12.50 in

$\therefore P_{cr} = \pi^2 \times 930.16 \times 10^3 / 12.50^2 = 58754$ kips $>> P_u$ ok.

$\rightarrow$ The column webs do not have a stability problem.

- **Shear reinforcement for the column webs**

Theoretically, the column webs do not need any shear reinforcement because all column shear will be concentrated above and below the captive beam portion. However, minimum required shear reinforcement should be provided to prevent the web rebars from local buckling and to account for the "compatibility shear" which arises when the connection deforms as a unit.

$\therefore$ Use DB4 ties at maximum spacing S_{max}

From Subsection 7.10.5 of ACI 318-89,

S_{max} = min(16 x long. rebar dia., 48 x tie dia., least dia. of each web)

= min(16 x 10/8 =20", 48 x 4/8 = 16", 7") = 7 in.

→ Use DB4 ties @ 7 in. spacing.

2.4.3 Design of Exterior MAPT Connections

Figure 2-6 shows the strut-and-tie model for the exterior MAPT connections. Techniques similar to those used with the regular MAPT model are applied when constructing the exterior strut-and-tie model.

- **Captive Beam Portion**

$C_f = C_d$ = 279.77 kips, from Fig. 2-6.

Compute T_n:

$T_n = C_f / 4\phi_D$, Eq. (3-2) from [2].

$\therefore T_n = 279.77 / (4 \times 0.85) = 82.29$ kips

Calculate A_S:

$A_s = kT_n / f_Y$,and k = 2 for diagonal compressive struts.

$A_s = 2 \times 82.29 / 60 = 2.74$ in^2.

Reinforce the splitting tensile forces with a pair of DB6 diagonal rebars with 60° inclination angle measured from horizontal axis, and compute for the amount of horizontal and vertical reinforcement, using Eqs. (3-14) and (3-15) from [2]:

$A_{sh} = (2.74 - (2 \times 0.44) \times \cos(90 + \alpha - 2\theta_3)) \sin(\theta_3)$;

$\alpha = \theta_3 - 60$.

$\therefore A_{sh} = (2.74 - 0.63) \sin(\theta_3) = 2.03$ in^2.

Similarly,

$\therefore A_{sv} = (2.74 - 0.63) \cos(\theta_3) = 0.57$ in^2.

→ Use 5 DB4 horizontal stirrups for $A_{sh} = 2.00$ in^2.
→ Use 2 DB4 vertical stirrups within the center portion for $A_{sv} = 0.80$ in^2.

Intermediate longitudinal rebars are not used due to possible construction difficulty.

- **Reinforcement for Column Portions Immediately Above and Below the Beam**

$C_f = C_d$ = 112.34 kips, from Fig. 2-6.

Compute T_n:

$T_n = C_f / 4\phi_D$, Eq. (3-2) from [2].

$\therefore T_n = 112.34 / (4 \times 0.85) = 33.04$ kips

Calculate A_S:

$A_s = kT_n / f_Y$,and k = 1 for vertical compressive struts.

$A_s = A_{sh} = 1 \times 33.04 / 60 = 0.55 \text{ in}^2$.

→ Use 2 DB4 horizontal stirrups within 10" distance above and below the captive beam portion; 10" being approximately the length of the vertical compressive struts, Fig. 2-6.

$\therefore A_{sh} = 0.80 \text{ in}^2$.

- **Column Webs**

From Section 10.3 of ACI 318-89,

$P_{u,max}$ of column $= 0.80\phi_c [0.85f'_c (A_g - A_{st}) + f_Y A_{st}]$

where $P_{u,max}$ = maximum allowable factored design axial load,
A_g = gross sectional area of column, and
A_{st} = total longitudinal steel area in the column section.

For each column web,

$P_u = 0.50 \times 701.13 = 350.57$ kips

$A_g = 7 \times 16 = 112 \text{ in}^2$.

$A_{st} = 3 \times$ Area of DB8 $= 3 \times 0.79 = 2.37 \text{ in}^2$.

$\therefore P_{u,max} = 0.80 \times 0.70 \times [0.85 \times 4000/1000 \times (112 - 2.37) + 60 \times 2.37]$

$= 288.37 \text{ kips} < P_u$ Nok.

Add 1-DB8 at each outer corner of the web,

→ $A_{st} = 3 \times 0.79 + 2 \times 0.79 = 3.95 \text{ in}^2$.

$\therefore P_{u,max} = 0.80 \times 0.70 \times [0.85 \times 4000/1000 \times (112 - 3.95) + 60 \times 3.95]$

$= 338.45 \text{ kips} \approx P_u$ ok.

- **Stability of Column Webs**

As with the example for regular MAPT connections, the column webs do not have a stability problem.

- **Shear reinforcement for the column webs**

With reasoning similar to the example for the regular MAPT connections:

→ Use DB4 ties @ 7 in. spacing

2.4.4 Reinforcement Details

Reinforcement details for the MAPT beam and column assemblies are shown in Figs. 2-7 and 2-8. Construction clearances of 0.50 in., for grouting interfaces, are provided by offsetting the column dimensions at the column bottoms and at the column slots. Also, the additional longitudinal

reinforcement for the column webs is looped under the column slots to facilitate the development of the reinforcement in compression.

2.4.5 Design of Beams and Columns for ANT Assemblies

A) Beam B1

- **Initial Parameters**

assumed beam dimensions	= 10 x 20	in.
assumed column depth	= 20	in.
largest reinforcement size (bundled in groups of 3)	= DB6	
estimated tensile development length	= 25	in.
dist. from column faces to DHLs	= 25	in.
factored design moment at left DHL section	= 1460.80	kip-in.
factored design moment at right DHL section	= 1348.77	kip-in.
factored design moment at left CF section	= 1816.39	kip-in.
factored design moment at right CF section	= 1603.95	kip-in.

- **Left and Right DHL Sections**

Try:

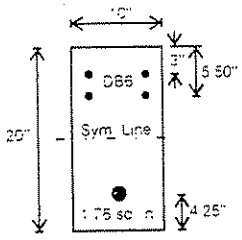

$f'_c = 6000$ psi., $f_Y = 60$ ksi.

$E_c = 4415$ ksi., $E_s = 29000$ ksi.

$\beta_1 = 0.85 - 0.05 \times (f'_c - 4000) / 1000 = 0.75$

$\rho = \rho' = A_s/bd = 11.17 \times 10^{-3} \geq \rho_{min} = 3.3 \times 10^{-3}$

$\rho < 0.75\rho_b = 28.3 \times 10^{-3}$ ok.

Assume tensile steel yields and compressive steel does not; then,

$\varepsilon_s' = 0.003\ (c - 4.25) / c = 0.003 - 12.75 \times 10^{-3} / c$

$\varepsilon_s = 0.003\ (15.75 - c) / c = 47.25 \times 10^{-3} / c - 0.003$

$C_1 = 0.85\ f'_c\ b\ \beta_1 c = 0.85 \times 6 \times 10 \times 0.75c = 38.25c$

$C_2 = A_s'\ E_s\ \varepsilon_s' = 153.12 - 650.76 / c$

$T = A_s\ f_Y = 1.76 \times 60 = 105.60$ kips

Solve: $c = 3.55$ in., $\varepsilon_s' = -0.591 \times 10^{-3}$, $\varepsilon_s = 10.310 \times 10^{-3} > \varepsilon_Y$

$C_1 = 135.79$ kips, $C_2 = -30.19$ kips (tension), $T = 105.60$ kips

$M_n = 1610.73$ kip-in., $\phi_b M_n = 1449.66$ kip-in. $\approx M_u$ ok.

To account for the potential strain hardening, assume $f_Y = 1.25 \times 60 = 75$ ksi.

Solve: $c = 3.86$ in., $\varepsilon_s' = -0.305 \times 10^{-3}$, $\varepsilon_s = 9.248 \times 10^{-3} > \varepsilon_Y$

$C_1 = 147.56$ kips, $C_2 = -15.56$ kips (tension), $T = 132.00$ kips

$M_n = 1931.66$ kip-in.

At left DHL section, overstrength factor due to strain hardening

$(O_e) = M_n/M_u = 1931.66 / 1460.80 = 1.322$

At right DHL section, $O_e = 1931.66 / 1348.77 = 1.432$

- **Left and Right CF Sections**

Try:

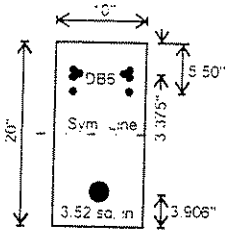

$f'_c = 6000$ psi., $f_Y = 60$ ksi.

$E_c = 4415$ ksi., $E_s = 29000$ ksi.

$\beta_1 = 0.85 - 0.05 \times (f'_c - 4000) / 1000 = 0.75$

$\rho = \rho' = A_s/bd = 21.87 \times 10^{-3} \geq \rho_{min} = 3.3 \times 10^{-3}$

$\rho < 0.75\rho_b = 28.3 \times 10^{-3}$ ok.

Assume tensile steel yields and compressive steel does not; then,

$\varepsilon_s' = 0.003 (c - 3.906) / c = 0.003 - 11.718 \times 10^{-3} / c$

$\varepsilon_s = 0.003 (16.094 - c) / c = 48.282 \times 10^{-3} / c - 0.003$

$C_1 = 0.85 f'_c b \beta_1 c = 0.85 \times 6 \times 10 \times 0.75c = 38.25c$

$C_2 = A_s' E_s \varepsilon_s' = 306.24 - 1196.17 / c$

$T = A_s f_Y = 3.52 \times 60 = 211.20$ kips

Solve: $c = 4.49$ in., $\varepsilon_s' = 0.388 \times 10^{-3}$, $\varepsilon_s = 7.762 \times 10^{-3} > \varepsilon_Y$

$C_1 = 171.60$ kips, $C_2 = 39.60$ kips, $T = 211.20$ kips

$M_n = 2955.68$ kip-in., $\phi_b M_n = 2660.11$ kip-in.

To ensure that plastic hinges will not form at the CF sections, the moment strength of the CF sections must be larger than upgraded design moment.

At left CF section, $\phi_b M_n > O_e M_u = 1.322 \times 1816.39 = 2401.27$ kip-in. ok.

At right CF section, $\phi_b M_n > O_e M_u = 1.432 \times 1603.95 = 2296.86$ kip-in. ok.

- **Shear Reinforcement**

1) Within Two Beam Depths from Column Faces (Section 21.9 ACI 318-89)

$V_u = 2M_{n\,@\,CF} / L_n$; L_n = clear span length = span length - column width

$= 2 \times 2955.68 / (300 - 20) = 21.11$ kips

or $V_u = V_{u,2E} \approx (2V_u)$ governing EQ Load case

$= 2 \times 14.58 = 29.16$ kips ← governs

$V_c = 2 (f'_c)^{1/2} bd / 1000 = 2 (4000)^{1/2} \times 10 \times (20 - 3.906) / 1000 = 20.36$ kips

Use DB4 stirrups @ max. allow. spacing S_{max}:

$S_{max} = \min (0.25d = 4.02", 8d_b = 8 \times 6/8 = 6", 24 \times$ dia. Stirrups $= 12", 12") = 4$ in.

$\therefore V_s = A_v f_y d / S_{max} = 0.40 \times 60 \times 16.094 / 4 = 96.56$ kips

$\phi V_n = \phi(V_c + V_s) >> V_u$ ok. → use DB4 stirrups @ 4 in. spacing.

2) Outside Two Beam Depths from Column Faces (Section 11.5 ACI 318-89)

$V_u = 14.58$ kips

The sections have enough shear capacity, therefore, use DB4 stirrups @ max. allowable spacing

$S_{max} = 0.50d = 8.05" \approx 8$ in.

B) Beam B2

The design loads of Beams B1 and B2 are roughly identical; therefore, use identical beam sections for both beams.

C) Column C1

- **Initial Parameters**

assumed column dimensions	= 18 x 18 in.
largest reinforcement size	= DB8

- **All Column Sections**

Try:

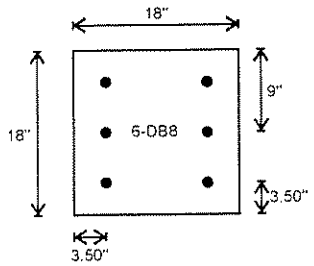

$f'_c = 6000$ psi., $f_Y = 60$ ksi.

$E_c = 4415$ ksi., $E_s = 29000$ ksi.

$\beta_1 = 0.75$, $\phi_c = 0.70$, $\phi_b = 0.90$

$A_s = 4.74$ in.^{2}, $A_g = 324$ in.^{2} → $A_s/A_g = 0.0146 > 0.01$ ok.

Gravity Load Case: $P_u = 845.98$ kips, $M_u \approx 0$ kip-in.

EQ. Load Case: $P_u = 701.13$ kips, and

$M_u = 2029.12$ kip-in. ← governs

or $P_u = 701.13$ kips, and

$M_u = (0.50\ O_e M_u)$@ left end of beam B1

$= 0.50 \times 1.339 \times 1961.38$

$= 1313.14$ kip-in.

From the interaction curve (Fig. 2-9a), this assumed section is adequate for column C1.

- **Shear Reinforcement**

1) Within the Length L_o from Joint Faces (Section 21.9 ACI 318-89)

L_o = max($H_n/6$, b_c, h_c);

H_n = clear column height = 120 - 20 = 100 in.; $H_n/6$ = 16.66 ≈ 17 in.;

b_c = column width = 18 in.,

h_c = column depth = 18 in.

$V_u = 2M_{n\,@\,joint\,face} / h_n$; use $M_n = M_{n,balance}$ = 3336 kip-in.

= 2 x 3336 / 100 = 66.72 kips ← governs

or $V_u = V_{u,2E} \approx (2V_u)$ governing EQ Load case

= 2 x 19.92 = 39.84 kips

$V_c = 2 (f'_c)^{1/2} b_c d_c / 1000 = 2 (6000)^{1/2}$ x 18 x (18 - 3.50) / 1000 = 40.43 kips

Use DB4 ties @ max. allowable spacing S_{max}:

S_{max} = min ($8d_b$ = 8 x 1= 8", 24 x dia. Stirrups = 12", $0.50h_c$ = 9", 12") = 8 in.

$\therefore V_s = A_v f_Y d / S_{max}$ = 0.40 x 60 x (18-3.50) / 8 = 43.50 kips

$\phi V_n = \phi(V_c+V_s)$ = 0.85(40.43+43.50) = 71.34 kips > V_u ok.

$\therefore$ use DB4 ties @ 8" spacing.

2) Outside the Length L_o (Section 11.5 ACI 318-89)

V_u = 19.92 kips

The sections have enough shear capacity; therefore, after the distance of 17" from joint faces, use DB4 ties @ max. allowable spacing

$S_{max} = 0.50h_c$ = 9" ≈ 8 in.

D) Column C2

- **Initial Parameters**

assumed column dimensions	= 20 x 20 in.
largest reinforcement size	= DB8

- **All Column Sections**

Try:

$f'_c = 6000$ psi., $f_Y = 60$ ksi.

$E_c = 4415$ ksi., $E_s = 29000$ ksi.

$\beta_1 = 0.7$, $\phi_c = 0.70$, $\phi_b = 0.90$

$A_s = 4.74$ in.^{2}, $A_g = 400$ in.^{2} → $A_s/A_g = 0.0118 > 0.01$ ok.

Gravity Load Case: $P_u = 1133.20$ kips, $M_u \approx 0$ kip-in.

EQ. Load Case: $P_u = 849.87$ kips, and

$M_u = 3203.41$ kip-in. ← governs

or $P_u = 849.87$ kips, and

$M_u = (0.50\ O_e M_u)$approx. @ left end of beam B1

$= 0.50 \times 1.339 \times 1961.38$

$= 1313.14$ kip-in.

From the interaction curve (Fig. 2-9b), this assumed section is adequate.
∴ use this assumed section for column C2.

- **Shear Reinforcement**

1) Within the Length L_o from Joint Faces (Section 21.9 ACI 318-89)

$L_o = \max(H_n/6, b_c, h_c)$;

H_n = clear column height = 120 - 20 =100 in.; $H_n/6 = 16.67 \approx 17$ in;

b_c = column width = 20 in.,

h_c = column depth = 20 in.

$V_u = 2M_{n\ @\ \text{joint face}} / h_n$; use $M_n = M_{n,\text{balance}} = 4512$ kip-in.

$= 2 \times 4512 / 100 = 90.24$ kips ← governs

or $V_u = V_{u,2E} \approx (2V_u)$ governing EQ Load case

$= 2 \times 32.85 = 65.70$ kips

$V_c = 2 (f'_c)^{1/2} b_c d_c / 1000 = 2 (6000)^{1/2} \times 20 \times (20 - 3.50) / 1000 = 51.12$ kips

Use DB4 ties @ max. allowable spacing S_{max}

$S_{max} = \min (8d_b = 8 \times 1 = 8", 24 \times \text{dia. Stirrups} = 12", 0.50h_c = 10", 12") = 8$ in.

∴ $V_s = A_v f_Y d / S_{max} = 0.40 \times 60 \times (20-3.50) / 8 = 49.50$ kips

$\phi V_n = \phi(V_c+V_s) = 0.85(51.12+49.50) = 85.53$ kips $\approx V_u$ ok.

∴ use DB4 ties @ 8" spacing.

2) Outside the Length L_O (Section 11.5 ACI 318-89)

$V_u = 32.86$ kips

The sections have enough shear capacity; therefore, use DB4 ties @ approx. max. allow. spacing

$$S_{max} = 0.50h_c = 10 \text{ in.} \approx 8 \text{ in.}$$

2.4.6 Design of Regular ANT Connection

Figure 2-10 depicts the strut-and-tie model for the regular ANT connections. The average locations of points of contraflexure are used for the beam portions of the strut-and-tie model, and the points of contraflexure for the column portions are assumed at the column mid-heights. The applied shear forces at the ends of the beam portions are assumed equal to the larger upgraded design moments at the beam CF sections, divided by the distances from the CF sections to the end of the beam portions.

- **Design of Connection**

$C_d = 503.13$ kips, from Fig. 2-10.

Try reinforcing the diagonal compressive strut with one pair of DB6 diagonal rebars at a 45° inclination angle measured from horizontal axis.

Apply Eq. (3-7) from [2]:

$C_f = 503.13 - 0.85 \times (2 \times 0.44) \times 60 \times \cos(\theta_3 - 45)$; $\theta_3 = 61.15°$, see Fig.2-10.

$\therefore C_f = 503.13 - 43.11 = 460.02$ kips

Compute T_n:

$T_n = C_f / 4\phi_D$, Eq. (3-2) from [2].

$\therefore T_n = 460.02 / (4 \times 0.85) = 135.30$ kips

Calculate A_S:

$A_s = kT_n / f_Y$, and k = 2 for diagonal compressive struts.

$A_s = 2 \times 135.30 / 60 = 4.51$ in^2.

Reinforce the splitting tensile forces with another pair of diagonal rebars crossing the first pair, and compute the amount of horizontal and vertical reinforcement, using Eqs. (3-14) and (3-15) from [2]:

$A_{sh} = (4.51 - (2 \times 0.44) \times \cos(90 + \alpha - 2\theta_3)) \sin(\theta_3)$;

$\alpha = \theta_3 - 45°$.

$\therefore A_{sh} = (4.51 - 0.85) \sin(\theta_3) = 3.21$ in^2.

Similarly,

$\therefore A_{sv} = (4.51 - 0.85) \cos(\theta_3) = 1.77 \text{ in}^2.$

→ use 6 DB4 horizontal stirrups plus 2 pairs of DB4 intermediate long. rebar layers for: $A_{sh} = 3.20 \text{ in}^2.$

→ use 5 DB4 vertical stirrups within the center portion for $A_{sv} = 2.00 \text{ in}^2.$

- **Reinforcement for Column Portions Immediately Above and Below the Beam**

$C_f = C_d = 160.57$ kips, from Fig. 2-10.

Compute T_n:

$T_n = C_f / 4\phi_D$, Eq. (3-2) from [2].

$\therefore T_n = 160.57 / (4 \times 0.85) = 47.23$ kips

Calculate A_S:

$A_s = kT_n / f_Y$,and k = 1 for vertical compressive struts.

$A_s = A_{sh} = 1 \times 47.23 / 60 = 0.79 \text{ in}^2.$

→ use 2 DB4 horizontal stirrups within 10" distance above and below the captive beam portion, 10" being approximately the length of the vertical compressive struts, Fig. 2-10, so that:

$\therefore A_{sh} = 0.80 \text{ in}^2.$

2.4.7 Design of Exterior ANT Connection

Figure 2-11 depicts the strut-and-tie model for the exterior ANT connections. Modeling techniques described for the regular connections are also applied for the exterior connections. The diagonal reinforcement is considered ineffective in reducing fanning of the diagonal compressive struts due to inadequate compressive development length inside the connections.

- **Captive Beam Portion**

$C_f = C_d = 296.92$ kips, from Fig. 2-11.

Compute T_n:

$T_n = C_f / 4\phi_D$, Eq. (3-2) from [2].

$\therefore T_n = 296.92 / (4 \times 0.85) = 87.33$ kips

Calculate A_S:

$A_s = kT_n / f_Y$,and k = 2 for diagonal compressive struts.

$A_s = 2 \times 87.93 / 60 = 2.91 \text{ in}^2.$

Reinforce the splitting tensile forces with a pair of DB6 45°-diagonal rebars, and compute for the amount of horizontal and vertical reinforcement, using Eqs. (3-14) and (3-15) from [2]:

$A_{sh} = (2.91 - (2 \times 0.44) \times \cos(90 + \alpha - 2\theta_3)) \sin(\theta_3)$;

$\alpha = \theta_3 - 45 = 22.03°$.

$\therefore A_{sh} = (2.91 - 0.82) \sin(\theta_3) = 1.93 \text{ in}^2$.

Similarly,

$\therefore A_{sv} = (2.91 - 0.82) \cos(\theta_3) = 0.82 \text{ in}^2$.

→ use 5 DB4 horizontal stirrups, so that: $A_{sh} = 2.00 \text{ in}^2$.
→ use 2 DB4 vertical stirrups within the center portion, so that $A_{sv} = 0.80 \text{ in}^2$.

Intermediate longitudinal rebars are not used due to a possible constructability problem.

- **Reinforcement for Column Portions Immediately Above and Below the Beam**

$C_f = C_d = 109.06$ kips, from Fig. 2-11.

Compute T_n:

$T_n = C_f / 4\phi_D$, Eq. (3-2) from [2].

$\therefore T_n = 109.06 / (4 \times 0.85) = 32.08$ kips

Calculate A_S:

$A_s = kT_n / f_Y$, and k = 1 for vertical compressive struts.

$A_s = A_{sh} = 1 \times 32.08 / 60 = 0.53 \text{ in}^2$.

→ use 2 DB4 horizontal stirrups within 10" distance above and below the captive beam portion, 10" being approximately the length of the vertical compressive struts, Fig. 2-11, so that:

$\therefore A_{sh} = 0.80 \text{ in}^2$.

2.4.8 Reinforcement Details

Reinforcement details for the ANT beam and column assemblies are shown in Figs. 2-12 and 2-13. Clearances required for the grouting interfaces are provided at each ANT connection by offsetting the column length of the columns by 1 in. (0.50 in. at the top and at the bottom).

2.4.9 Design of Corner ANT Assembly

A corner ANT assembly is essentially an exterior ANT assembly in two planes. Therefore, the design of components constituting a corner ANT assembly are similar to those for an exterior assembly.

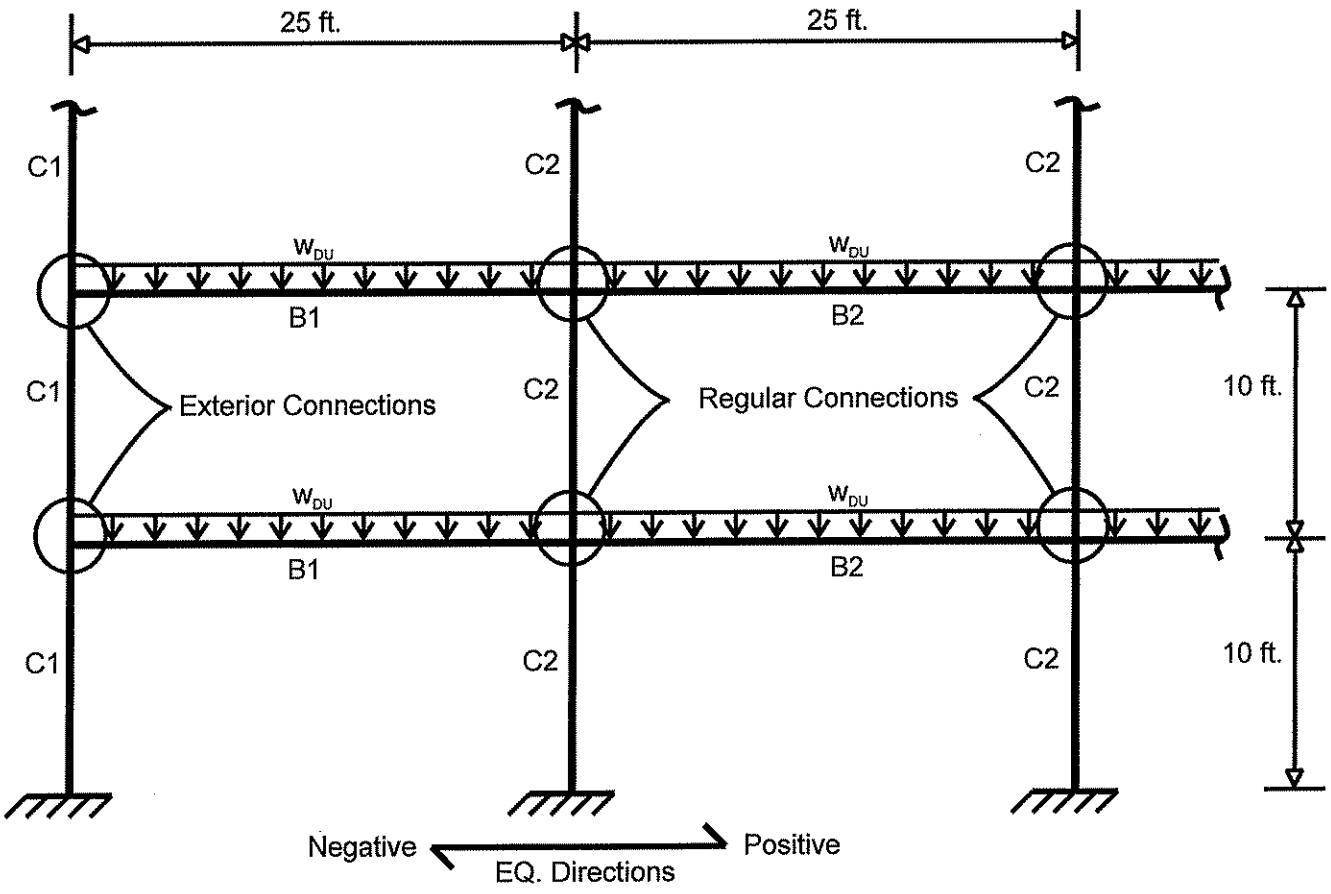

Figure 2-1 Portion of Frame for Design Example

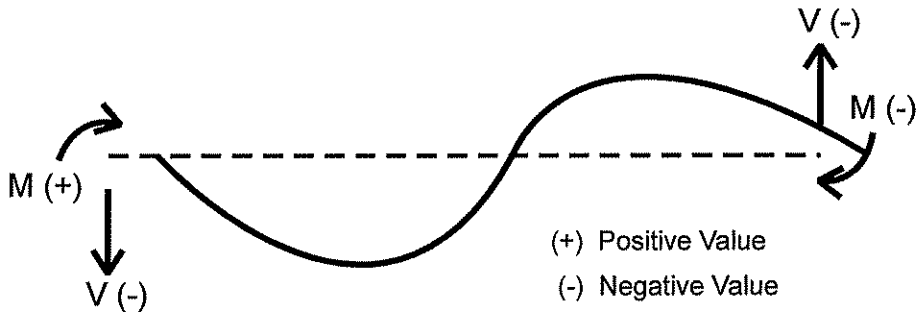

(a) Sign Conventions

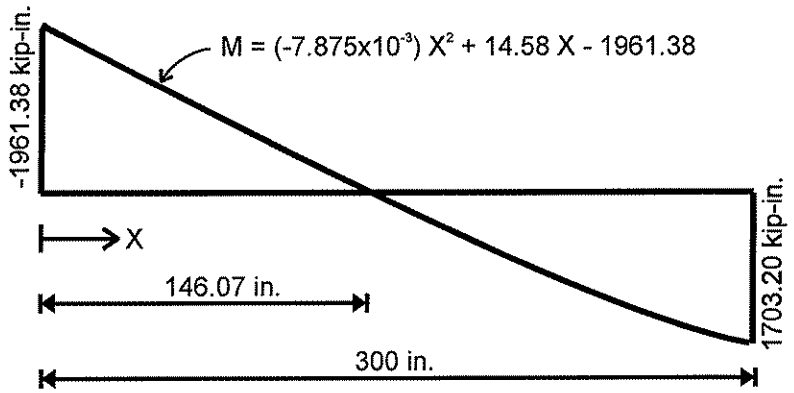

(b) Beams B1

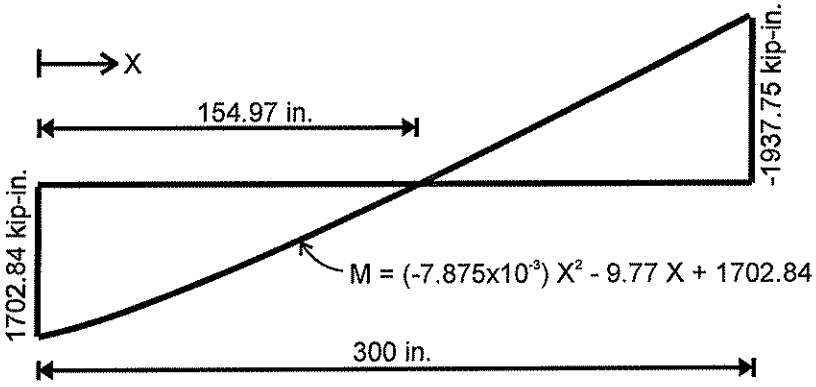

(c) Beams B2

Figure 2-2 Sign Conventions and Bending Moment Diagrams for Beam Designs

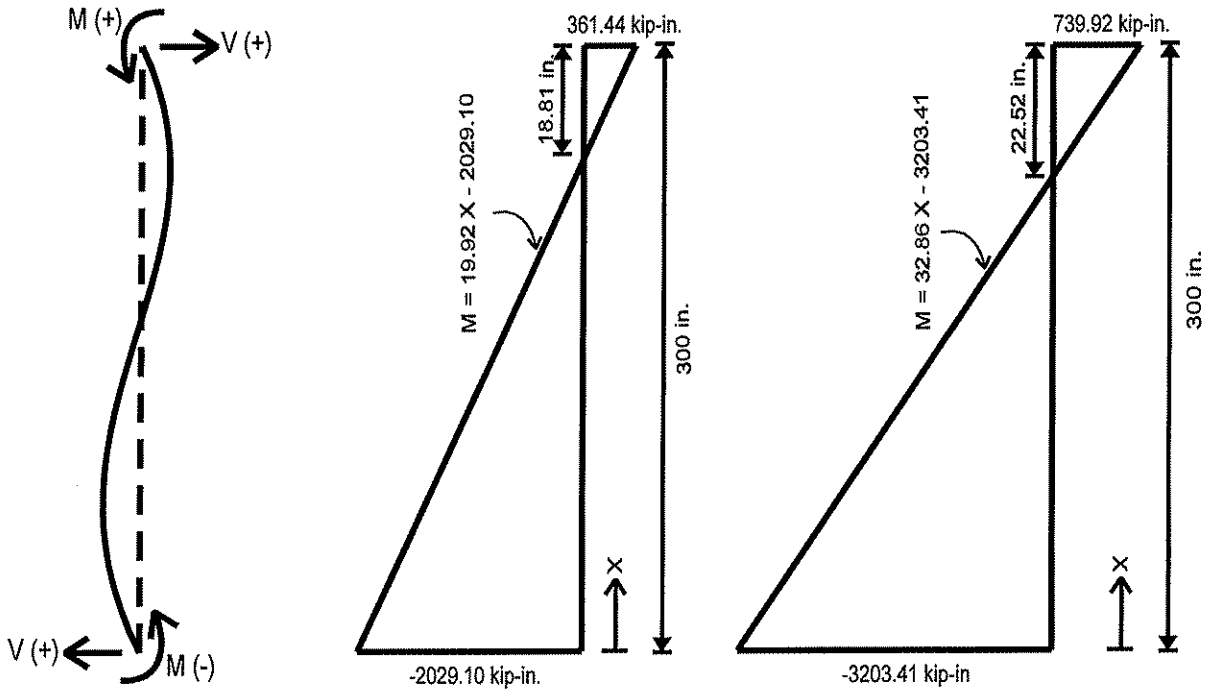

(a) Sign Conventions (b) Columns C1 (c) Columns C2

Figure 2-3 Sign Conventions and Bending Moment Diagrams for Column Designs

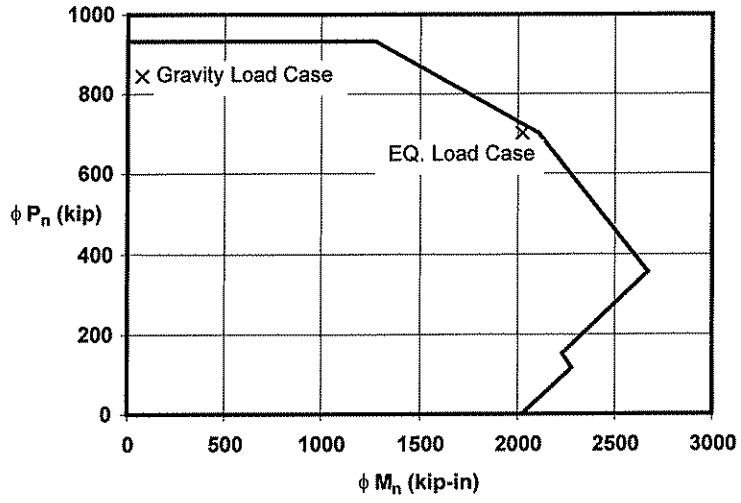

(a) Columns C1

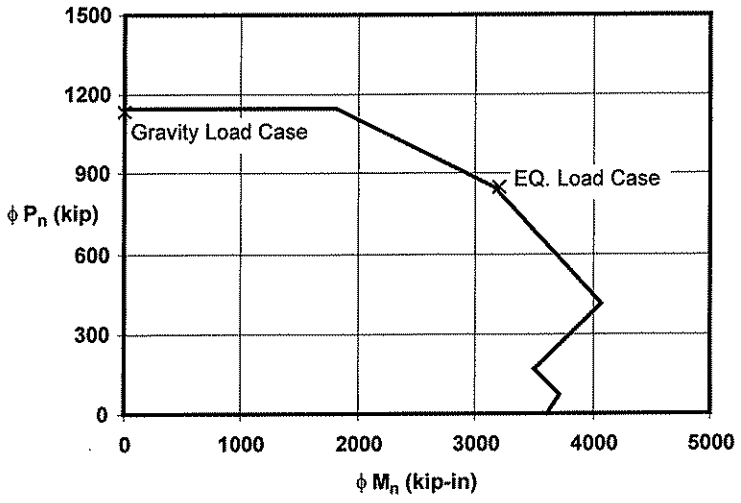

(b) Columns C2

Figure 2-4 Interaction Diagram for Columns of MAPT Assemblies

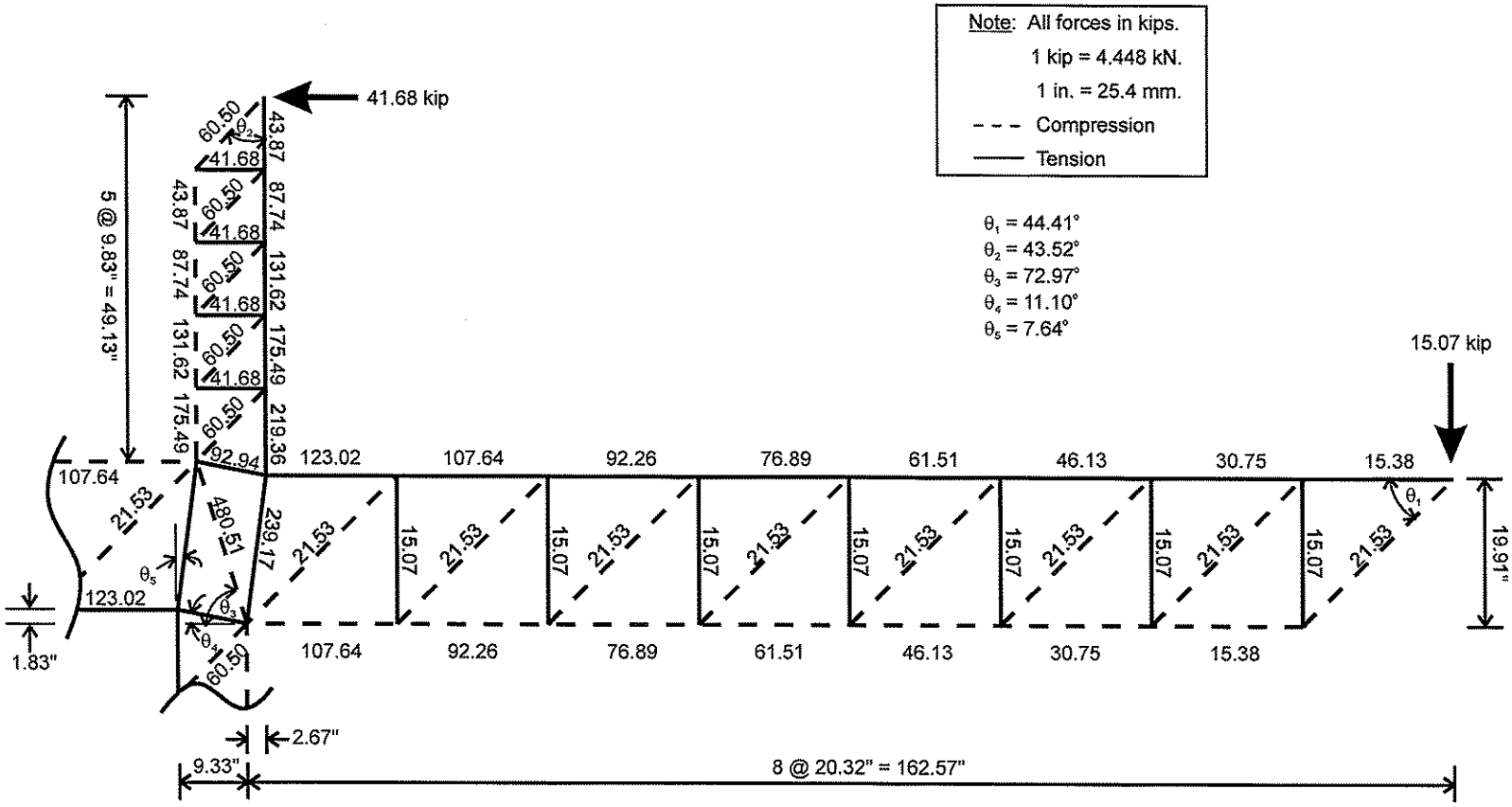

Figure 2-5 Strut-and-Tie Model for Regular MAPT Connections

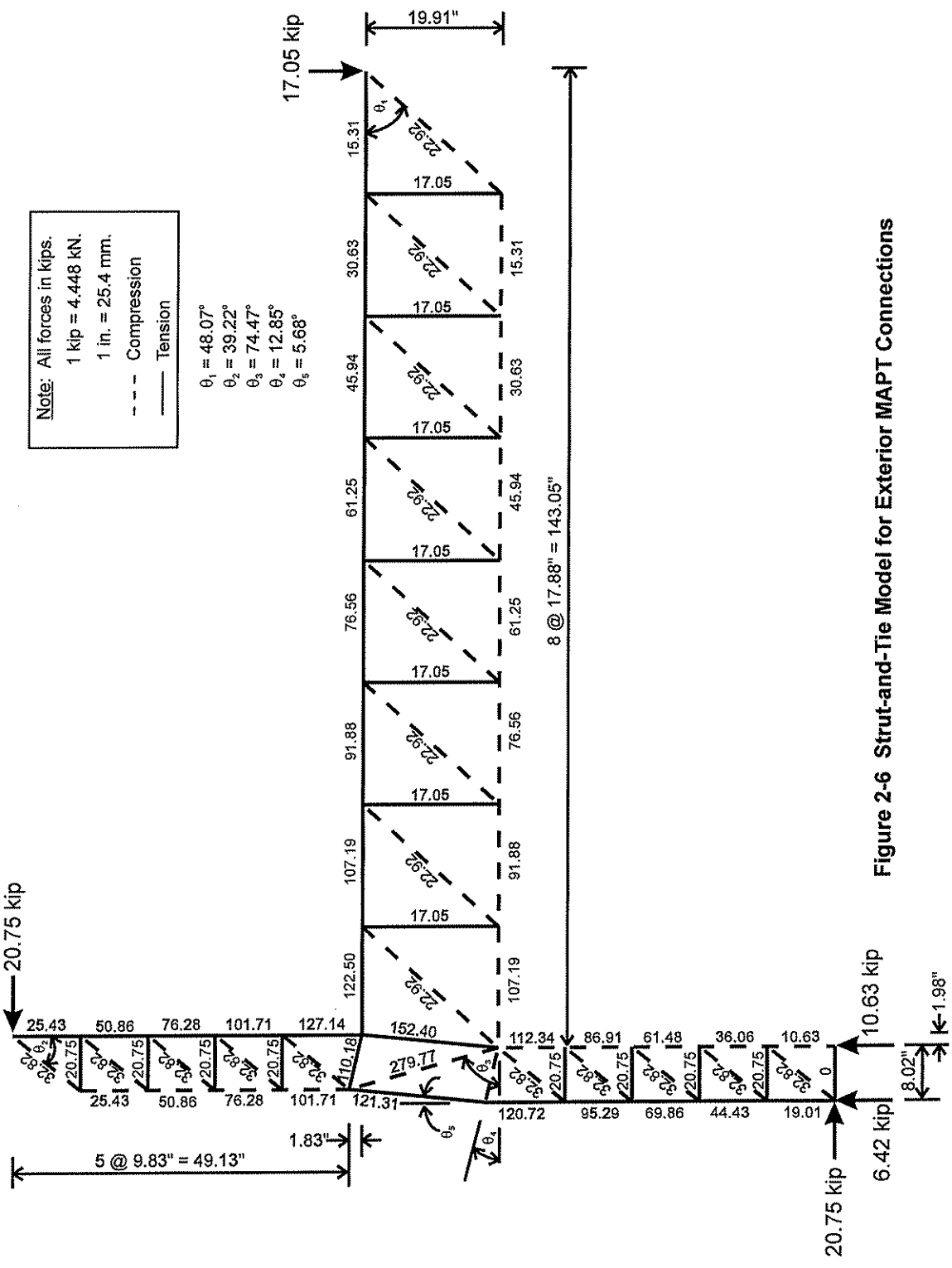

Figure 2-6 Strut-and-Tie Model for Exterior MAPT Connections

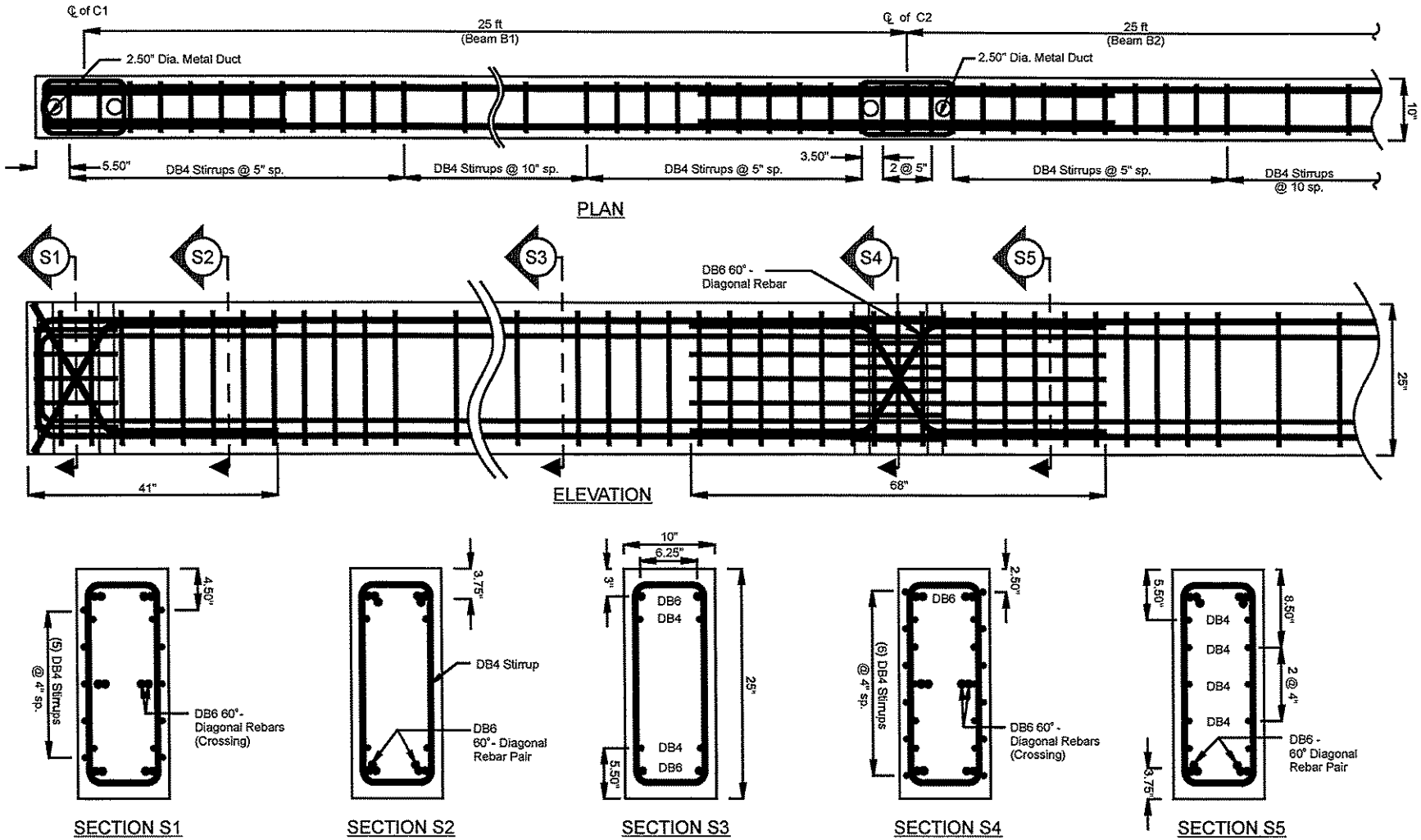

Figure 2-7 Reinforcement Details for MAPT Beam Assemblies

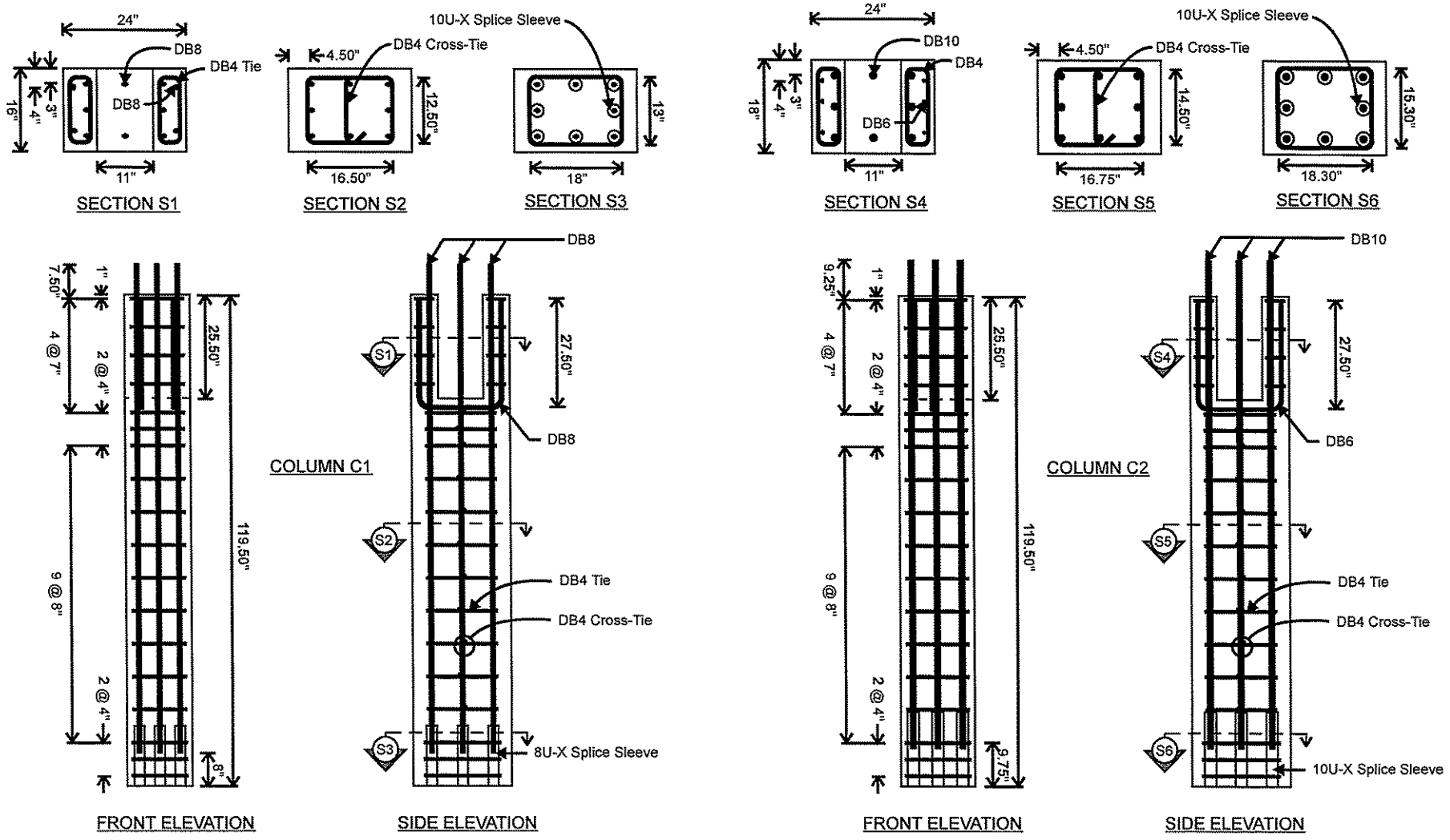

Figure 2-8 Reinforcement Details for MAPT Column Assemblies

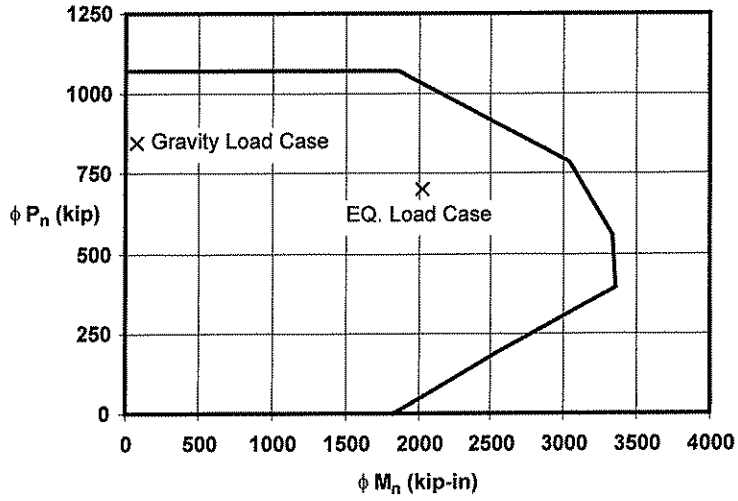

(a) Columns C1

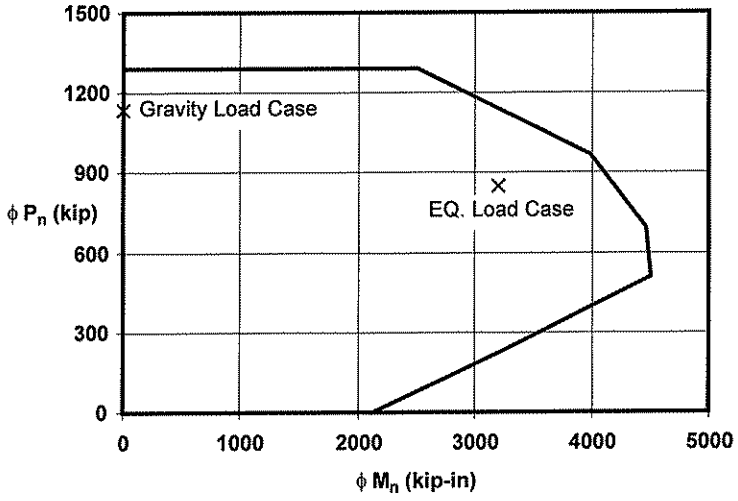

(b) Columns C2

Figure 2-9 Interaction Diagram for Columns of ANT Assemblies

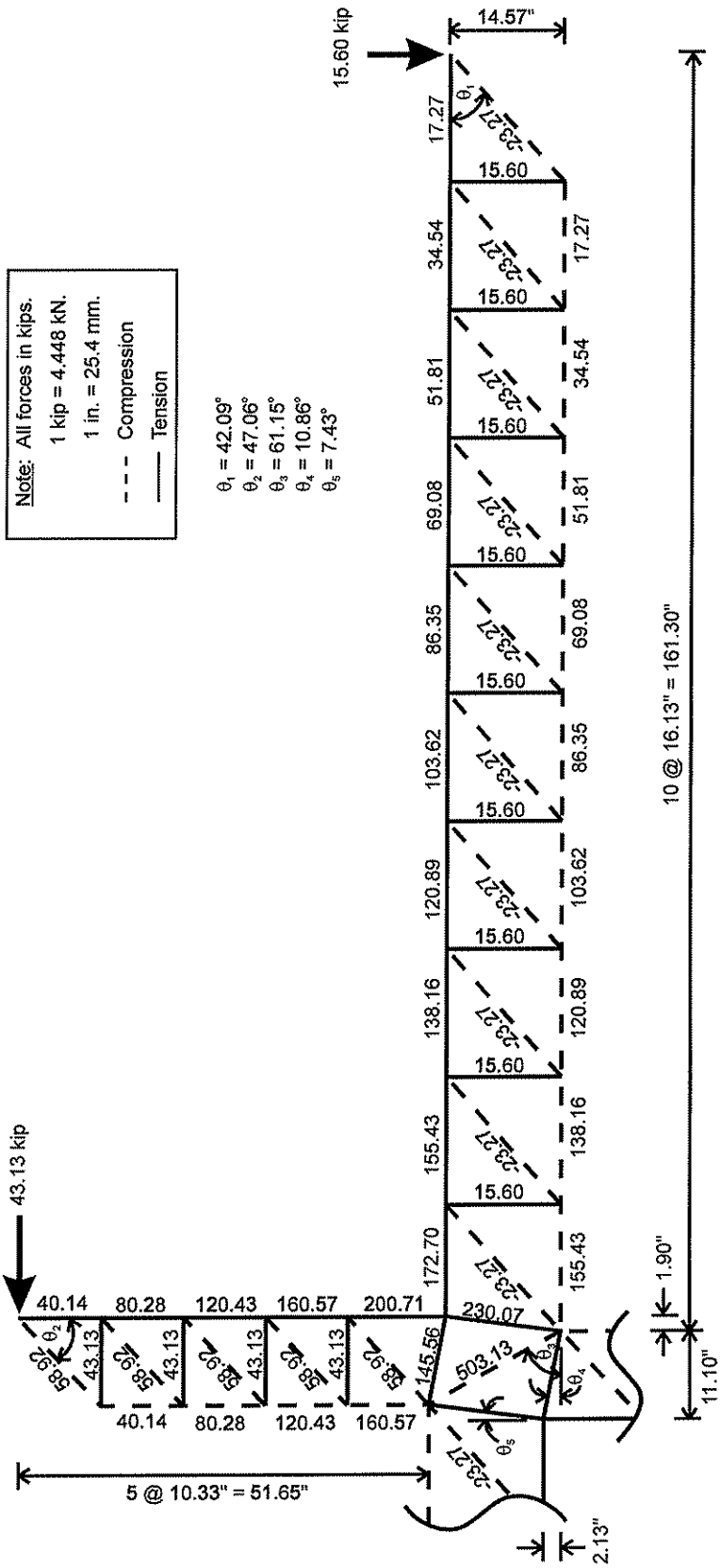

Figure 2-10 Strut-and-Tie Model for Regular ANT Connections

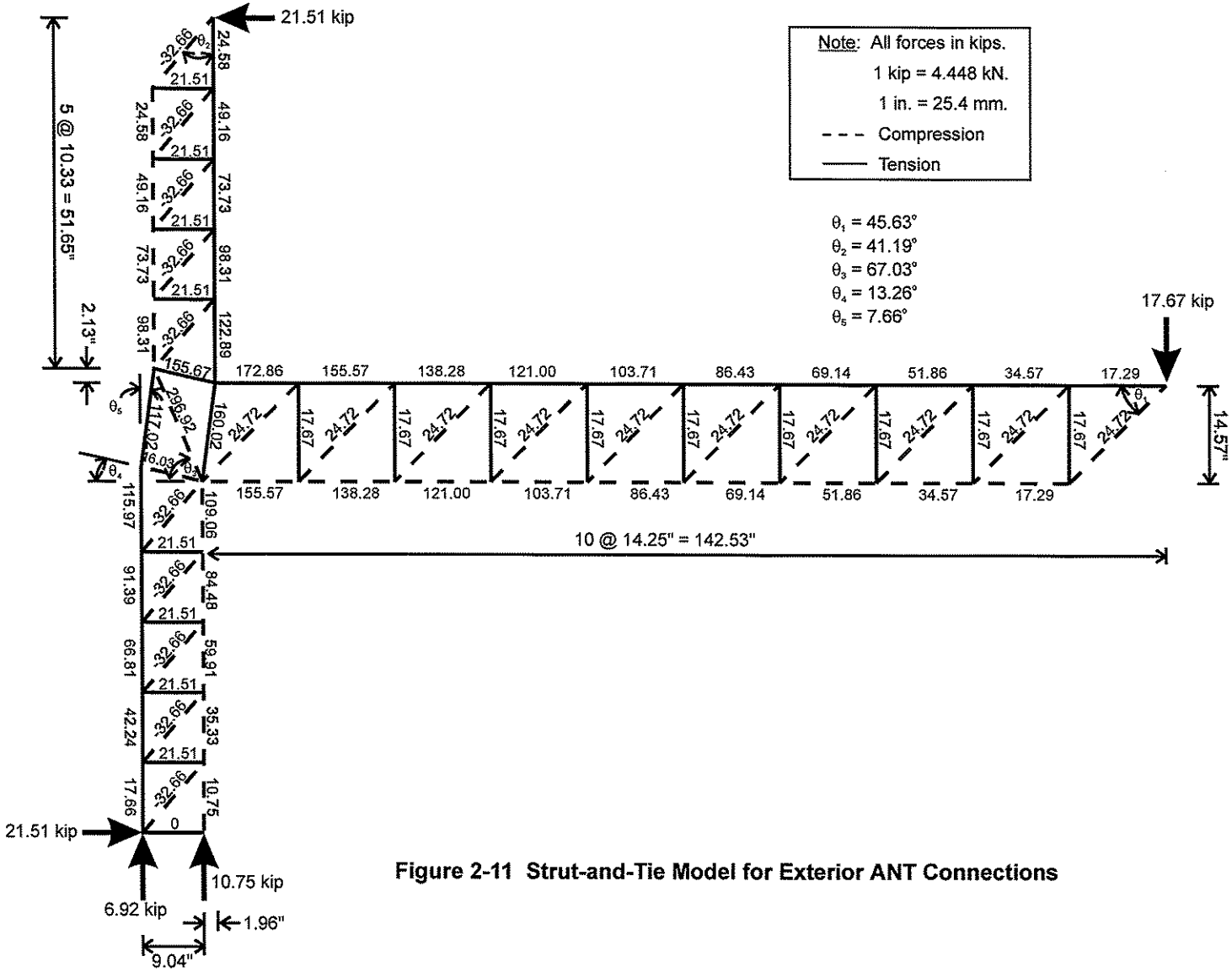

Figure 2-11 Strut-and-Tie Model for Exterior ANT Connections

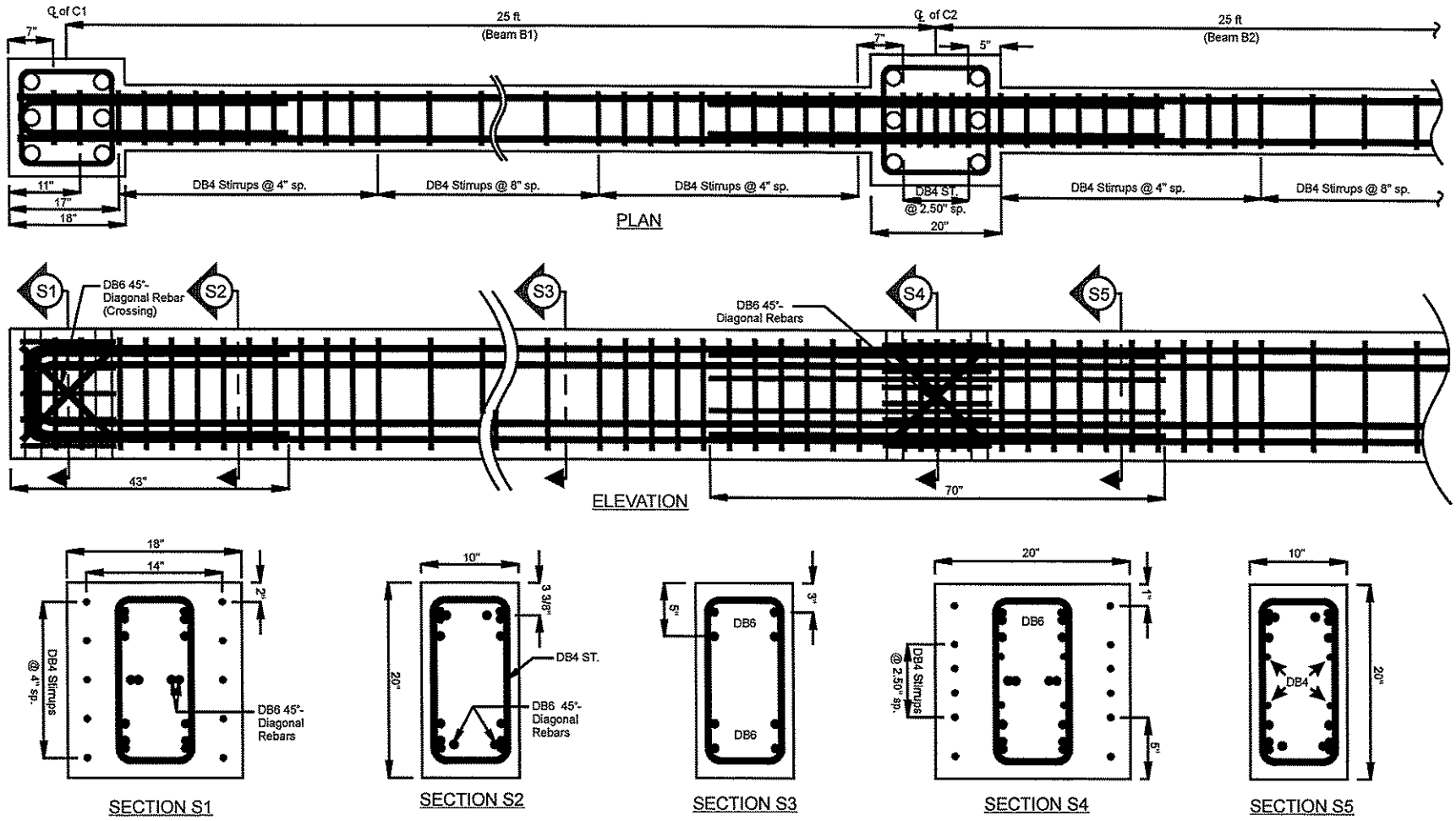

Figure 2-12 Reinforcement Details of ANT Beam Assemblies

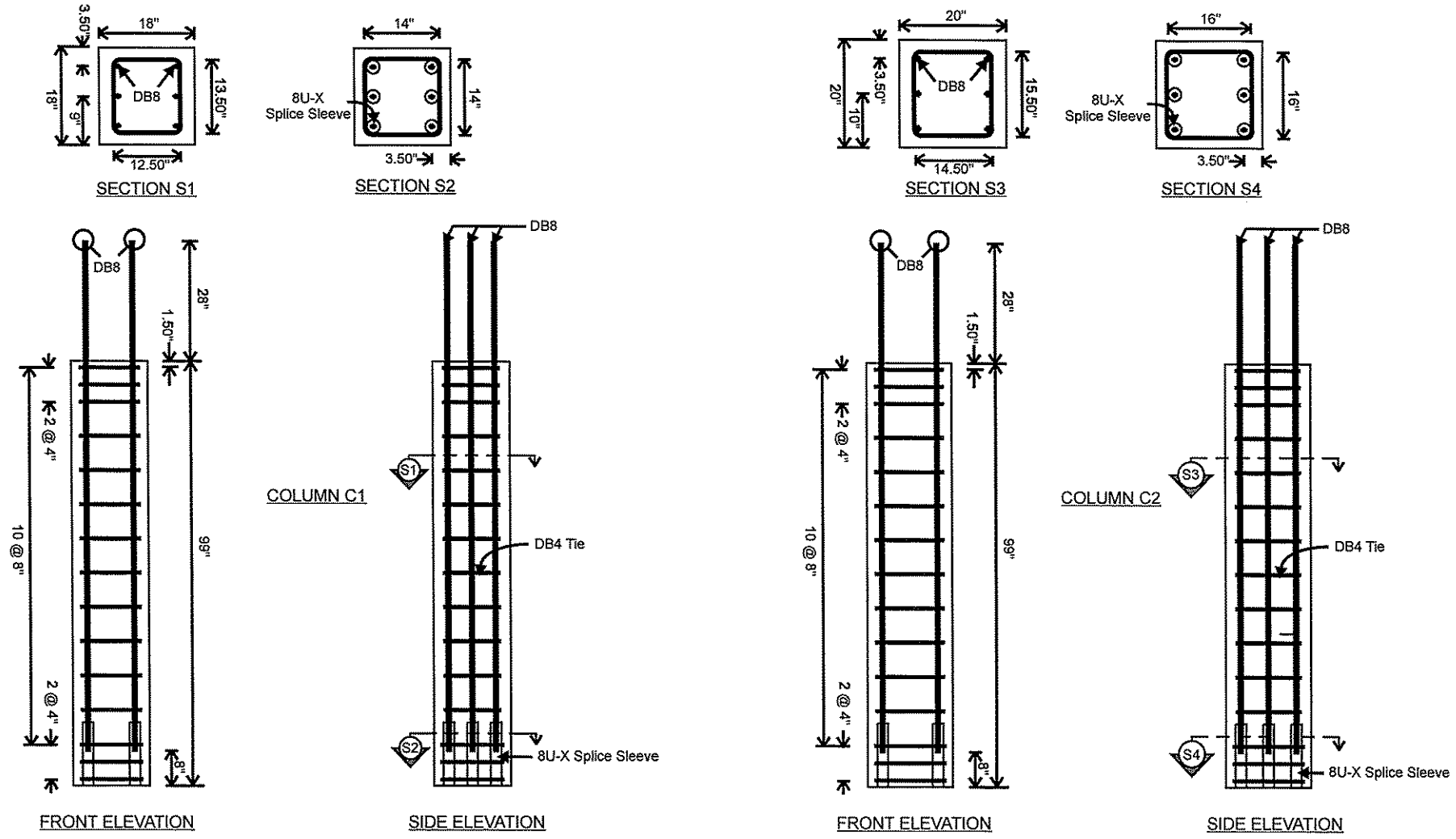

Figure 2-13 Reinforcement Details for ANT Column Assemblies

(This page is blank)

3. SEISMIC ANALYSES

Seismic response analyses were performed to evaluate the seismic adequacy of the design methodologies just described for APC systems. Inelastic static and inelastic dynamic analyses were conducted for two frame structures, one with MAPT beam-column connections and the other with ANT connections. In the inelastic static analyses, the frames were subjected to incremental seismic-equivalent lateral loads. Two lateral load patterns were used; UBC-specified and uniformly distributed. These load patterns were kept constant during the analyses, but the magnitudes of the loads were increased proportionally until failure occurred. In the inelastic dynamic analyses, the frames were subjected to two ground acceleration records; the first with a peak ground acceleration comparable to that of *typical* moderate earthquakes in the Northeastern United States and the second being consistent with severe California earthquakes. Computer software DRAIN-2DX [7] was used in performing both analyses.

The frame structures utilized are derived from the middle frame of the prototype structure used in developing the earlier experimental program [2]. The "MAPT frame" contains MAPT beam-column connections, and the "ANT frame" has ANT connections. Both frames were designed for a moderate seismic region (UBC zone 2A). The design of the beams, column, and beam-column connections of both frames was carried out using the design methodologies described earlier. A nominal concrete compressive strength of 4000 psi was used for the entire MAPT frame. For the ANT frame, a nominal concrete strength of 6000 psi was used for the lower three stories and 4000 psi was used for the upper five stories. The nominal yield strength of the steel reinforcement was 60 ksi for both frames.

Figure 3-1 shows the elevation of the frames and the member identifications. The DHL locations for both frames are summarized in Table 3-1. Cross-sections of the beams and columns are shown in Figs. 3-2 to 3-5.

Table 3-1 Designated Hinge Locations (DHLs) on MAPT and ANT Frames

Story	DHL Locations from Column Center on MAPT Frame		DHL Locations from Column Center on ANT Frame	
	Near Exterior Connections (in.)	Near Regular Connections (in.)	Near Exterior Connections (in.)	Near Regular Connections (in.)
(1)	(2)	(3)	(4)	(5)
Roof	30	32	32	33
7	30	32	32	33
6	33	34	33	34
5	33	34	33	34
4	33	34	33	34
3	33	34	34	35
2	33	34	34	35
1	33	34	34	35

3.1 Assumptions

To develop practical analytical models, the following assumptions and estimates for both frames were made:

1. **All beam-column connections are rigid connections, that is, they can displace but cannot deform.**

Justification: The design method for both MAPT and ANT connections is aimed at achieving strong connection behavior in which structural failure occurs away from the beam-column connections. Thus, it is reasonable to assume that the connections will remain undamaged during a seismic event, and remain much stiffer than the beams and columns framing into them. Most of the structural deformation, therefore, occurs in the beams and columns, and connection deformation can be safely neglected and the connection can be modeled as a rigid connection.

2. **The moment-curvature relationships of the beam sections of the MAPT and ANT frames are identical to those of the beam sections of the Group B specimens, when non-dimensionalized with respect to the yield moments and yield curvatures.**

3. **The moment-curvature relationships of the column sections, on the other hand, are of the elastic-perfectly plastic type.**

4. **Curvature and rotational ductility capacities of beam plastic hinges are equal to those of the beams of the Group B specimens having the same beam cross-sectional aspect ratios.**

5. **Curvature and rotational ductility capacities of column plastic hinges are obtained from cross-sectional analyses based on beam theory.**

Justification: The beam sections of both MAPT and ANT frames were designed using the design method identical to that of Group B specimens. Group B specimens had failures occurring in the beams at the plastic hinges. The moment-curvature relationships of the beam sections at the plastic hinges represent the complete behavior of the beam sections, from the initial loading stage to the failure stage. Toward the failure stage, the effects of concrete confinement, strain hardening and rebar buckling will modify the behavior of the beam sections. Experimentally obtained moment-curvature relationships, such as those of the beam sections of the Group B specimens, automatically take into account such effects. For the plastic hinges of the MAPT and ANT columns, however, elastic-perfectly plastic behavior was assumed due to the lack of experimental data. Cross-sectional analyses based on the beam theory assumptions were used. The effects of concrete confinement, strain hardening, and rebar buckling were ignored in the analyses, which should give conservative estimates of the curvature and rotational ductility capacities of the column plastic hinges.

6. **Yield moments and yield curvatures are estimated using the nominal concrete and steel properties. Sections are assumed cracked initially, thus the tensile strength of concrete can be omitted. Furthermore, confinement effects and strain hardening effects are ignored.**

Justification: Yield moments and yield curvatures are part of the ascending range of the moment-curvature relationships. For beams and columns in moderate seismic zones, it is expected that, at this stage, the confinement and strain hardening effects will not have a significant impact on the magnitudes

of the yield moments and yield curvatures, so that they can be estimated neglecting these effects. Additionally, beam and column sections of typical structures are likely to crack under normal loading conditions making it reasonable to neglect the contribution of concrete tensile strength when estimating the yield moment and yield curvature.

7. **Contribution of floor slabs to the beam stiffness is neglected.**

Justification: The prototype structure utilized total precast construction, in which precast floor slabs, with 2" thick unreinforced concrete topping, oriented parallel to the beams were used. It is unlikely that the precast slabs and the unreinforced topping will significantly contribute to the beam stiffness.

8. **Column stiffness, which depends on the magnitudes of the axial forces acting on the columns, is estimated using the axial forces induced under gravity loading.**

Justification: Theoretically, column stiffness should be estimated using the *real-time* magnitudes of the applied axial forces. This, however, requires that the structures be remodeled at every computational interval to account for the change in the magnitudes of the axial forces; an effort that will involve enormous computations and expense. To limit the computational effort, average and constant stiffness, instead of real-time stiffness, should be used. Due to the reversal nature of the earthquake motion and the likelihood that the structures will not exhaust their elastic restoring forces, the average magnitudes of the axial forces should be near to those induced by the gravity loads. The column stiffness was thus estimated in the analyses by using the axial forces resulting from gravity loading.

9. **The magnitudes of gravity loads on the structures when an earthquake occurs are approximated using the full amount of the unfactored design dead loads and one-quarter of the unfactored design live loads.**

Justification: It is unlikely that the structures will experience the full magnitude of design live loads when an earthquake occurs. It is estimated in this study that the full design dead loads plus 25% of the design live loads represents a realistic loading condition as the structure undergoes an earthquake event.

10. **Damping inherent during the elastic stage is approximated using a 5% viscous damping ratio.**

Justification: Wakabayashi [8] suggests that a 5% viscous damping ratio be used in performing dynamic analyses of reinforced concrete structures. Viscous damping was included in the dynamic analyses in the form of mass proportional and stiffness proportional coefficients (Rayleigh damping coefficients). Mathematical relationships between the viscous damping ratio and the Rayleigh damping coefficients are available from Clough and Penzien [9].

3.2 Seismic Load Patterns and Ground Acceleration Records

Two seismic-equivalent lateral load patterns were used in the inelastic static analyses. The first is specified in Section 2312(e) of the UBC code [10]. It resembles approximately an inverted triangular shape and represents the case when the first mode of vibration governs the seismic behavior. The second pattern assumes that the seismic force is distributed uniformly along the height of the structures. This uniformly distributed load pattern has its centroid closer to ground level than the UBC-specified pattern. Because the centroids of the inertia forces of the higher modes of vibration are normally lower than that of the first mode, the uniformly distributed load pattern represents somewhat the cases when the higher mode contributions are significant. In calculating the UBC-specified seismic load pattern, analytically

calculated fundamental periods of the frames were used because they were significantly larger than the periods computed from the UBC method. This point will be discussed further in Section 3.3.1.

Two ground acceleration records were utilized in the inelastic dynamic analyses, namely, the Nahanni and El Centro records (Fig. 3-6). The Nahanni record has been used by other investigators to study the seismic response of structures constructed in Northeastern United States, whereas the El Centro record represents a severe Californian earthquake. The power spectral densities of the Nahanni and El Centro earthquakes are shown in Fig. 3-7, normalized with respect to their peak values and plotted against the period content of the earthquake records.

The Nahanni acceleration was recorded at a site with hard soil to bed rock conditions and an epicentral distance of 23 km. The record corresponds to the horizontal North-South component of the earthquake and has a duration of about 19 sec. The peak ground acceleration (PGA) is approximately 0.148g, where g is gravitational acceleration. The Nahanni earthquake occurred on December 23, 1985. The El Centro record was obtained from the El Centro earthquake, on a stiff soil site. The El Centro earthquake occurred on May 18, 1940. The record lasts about 53 sec. and corresponds to the horizontal component in the North-South direction (S00E). The PGA value of the El Centro record is 0.348g. Only the first 20 sec. of the record is shown in Fig. 3-6 and used in the analyses. The remaining 33 sec. of the record has smaller ground acceleration values and does not have a significant impact on the results of the dynamic inelastic analyses.

3.3 Analytical and Modeling Techniques and Results

The beams and columns of both MAPT and ANT frames were modeled in the analyses using a series of beam-column elements (Type 2, Ref. [7]). Wu [11] did a series of studies on the accuracy of the DRAIN-2DX beam-column element and showed that the element works well in the elastic range. However, it works well in the inelastic range only when the element is in single curvature, especially with the ratio of end moments closer to unity. When the beam-column element is in the inelastic range and in double curvature, its performance degrades rapidly. The worst performance of the beam-column element occurs when the ratio of end moments approaches -1. To overcome this shortcoming, each beam was modeled using multiple beam-column elements. The lengths of the elements were such that those elements which were expected to experience yielding were always in single curvature, and only those which would remain elastic throughout were in double curvature. The ratio between the end moments of the elements which were expected to yield was kept roughly above 0.50. On the other hand, all columns except those of the first floor were expected to behave elastically; therefore, only one beam-column element was used in modeling each column. Two beam-column elements were used in modeling the first story columns, because they might yield at their bases.

In modeling the rigidity of the beam-column connections, the ends of the beam-column elements affixed to the connections were modeled as being rigid by activating the rigid end zone option [7] of the beam-column elements.

Gravity loads were modeled as nodal forces acting at the beam-column intersections. The gravity load effects were included in both the inelastic static and inelastic dynamic analyses, and also in the determination of the natural periods of the MAPT and ANT frames. In the elastic static analyses, gravity load effects were evaluated prior to applying the seismic equivalent loads or the ground accelerations.

The analyses were continued until failure occurred, failure being defined as the state at which the structures begin unloading. Unloading was assumed to occur when the maximum rotations at one or more simultaneously forming plastic hinges exceeded the rotational capacity. The rotational capacity of a plastic hinge is the product of the estimated yield rotation and the rotational ductility capacity. The

yield rotation was estimated as the analytically computed yield curvature multiplied by the plastic hinge length. Both the plastic hinge length, non-dimensionalized with respect to the beam depth, and the rotational ductility capacity were assumed to be identical to the average of those of the plastic hinges of the laterally braced Group B specimens. In the inelastic static analyses, load magnitudes were scaled up proportionally as the analyses progressed using a displacement control algorithm with a displacement increment of 0.10" per step.

In the inelastic dynamic analyses, three earthquake scenarios were included; moderate, severe, and largest sustainable. A moderate earthquake is one with a seismic activity PGA value of 0.15g to 0.20g. A severe earthquake has a PGA magnitude of 0.30g to 0.40g. The maximum sustainable earthquake was defined as one with a PGA that leads to failure of the frame structures. The Nahanni acceleration record, with a PGA of 0.148g is classified as a moderate earthquake. The El Centro record with a PGA of 0.348g represents a severe earthquake. The Nahanni record was scaled up by 2 to reach the level of severe earthquakes. Similarly, the El Centro record was scaled down by one-half to become a moderate earthquake. To find the largest sustainable earthquake, iterations were required to determine the multiplying factors to scale up the ground acceleration record. In the iteration process, a multiplying factor was projected based on previous analysis results, and an inelastic dynamic analysis was carried out using the projected factor. The required factor was determined when failure occurred. A time-history algorithm with a constant time step of 0.01 second was utilized in conducting the inelastic dynamic analyses.

The analyses were carried out in the following order. First, the natural periods of the MAPT and ANT frames were computed. Then inelastic static analyses were made using the UBC-specified and the uniformly distributed load patterns. Finally, inelastic dynamic analyses were conducted.

3.3.1 Natural Periods of MAPT and ANT Frames

Table 3-2 First Four Natural Periods of MAPT and ANT Frames

Frame	Periods of Original Frame				UBC Period	Periods of Redesigned Frame			
	1st (sec.)	2nd (sec.)	3rd (sec.)	4th (sec.)	(sec.)	1st (sec.)	2nd (sec.)	3rd (sec.)	4th (sec.)
(1)	(2)	(3)	(4)	(5)	(6)	(7)	(8)	(9)	(10)
MAPT (Cracked)	2.71	0.96	0.54	0.34	0.80	1.08	0.38	0.24	0.17
MAPT (Gross)	1.48	0.50	0.29	0.69		0.65	0.24	0.14	0.12
ANT (Cracked)	3.20	1.05	0.58	0.36	0.80	1.16	0.42	0.26	0.18
ANT (Gross)	1.80	0.60	0.34	0.22		0.72	0.26	0.16	0.13

Columns (2) to (5) in Table 3-2 list the first four computed periods of vibration of the MAPT and ANT frames based on the gross and "cracked" section properties, and Col. (6) shows the periods (first mode) computing using UBC. It can be seen that the fundamental periods of the frames based on cracked sections are larger than those based on gross sections and that both the gross and cracked section results are much larger than those given by UBC. Because the UBC equation for fundamental periods is in part based on measurements of actual building responses during small earthquakes, the structural members of

the buildings are uncracked or cracked to a minor degree. As a result, the periods computed using the UBC equations should be somewhat bracketed by the analytically calculated periods based on gross (uncracked) and cracked sections.

The orientation of the precast floor slabs in the prototype structure is probably primarily responsible for the large difference between the analytically computed first mode periods and the periods given by the UBC equation. The precast floor slabs of the prototype structure span parallel to the lateral load-resistant frames. As a result, the gravity loads on the structure, except the beam self-weight, are carried by the simply supported inverted T-beams in the direction perpendicular to the lateral load-resistant frames. The beams of the lateral load-resistant frames, therefore, carry only the seismic loads plus their own self-weight, thus resulting in relatively small values for the required beam and column dimensions. In contrast, the beams and columns of a similar lateral load-resistant frame of a CIP construction, or another precast frame, in which the precast slabs span between the lateral load-resistant frames, will be relatively larger, because the beams of these frames also have to carry part of the slab dead and live loads. Therefore, the frame in which the slabs run parallel to it will have less stiffness, and correspondingly longer natural periods, compared to other cases.

To assess the effect of the direction of the precast floor slabs, the periods of the MAPT and ANT frames were recomputed for the floor slabs being rotated 90°. To do this, the prototype structure first had to be redesigned. In this case, beams of the lateral load-resistant frames carry both the lateral loads and all the gravity loads. The redesign showed that in order to carry both the lateral and gravity loads, the beam sizes must be increased to about 15" x 50" for the MAPT and to 15" x 40" for the ANT frame. The corresponding increase of the flexural stiffness was about 12 times. In addition, due to the increase in the moment carrying capacity of the beams, the column sizes must be increased so that their flexural stiffness would be twice as large as originally. The results of the period recomputation are shown in Cols. (7) to (10) in Table 3-2. Comparison between Cols. (6) and (7) indicates that the analytically re-calculated first periods and the periods computed by the UBC equation are now in much closer agreement.

Because the computations for natural periods showed that the natural periods of the prototype structure were sensitive to the orientation of the precast floor slabs (the paths of the gravity load transfer), the issue of slab orientation will have to be taken into account in design, especially for low- to medium-rise structures. This result has an important implication in seismic-resistant design, because the fundamental period is required in calculating the design base shear. For building frames utilizing precast floor slabs, careful considerations must be given to the determination of the "design" natural period, especially when the structures have precast floor slabs spanning in the direction parallel to the seismic frames. As shown by the results herein, analytically calculated periods of structures can deviate significantly from code-specified values when the precast slabs run parallel to the seismic frames.

3.3.2 Inelastic Static Analyses

Figure 3-8 shows the relationships between base shear (sum of all lateral load at floor levels) and roof displacements of the MAPT and ANT frames obtained from the inelastic static analyses for the UBC-specified and the uniform lateral load patterns. The relationships are plotted up to frame failure (shown as points C in the figure), at which point the rotational capacity of one or more plastic hinges was exhausted. The locations of the plastic hinges at the onset of first yielding and at the load levels at which the last hinges formed are also shown, indicated as points A and B, respectively.

Table 3-3 compares the magnitudes of the factored design seismic loads for the MAPT and ANT frames to the yield and ultimate loads obtained from the inelastic static analyses. The factored design loads are listed for both UBC-specified periods and analytically calculated periods. The factored design

loads based on the UBC periods were used in the designs of the MAPT and ANT frames. In determining the values in Col. (3), the analytically calculated periods were used in the UBC base shear equations.

Table 3-3 Yield and Ultimate Strengths of MAPT and ANT Frames

Based on Inelastic Static Analyses

Frame and Analysis Method	Factored Design Base Shear			Yield Load			Ultimate Load		
	UBC Period (kip)	Analyt Period (kip)	(2)/(3)		(5)/(2)	(5)/(3)		(8)/(2)	(8)/(3)
(1)	(2)	(3)	(4)	(kip) (5)	(6)	(7)	(kip) (8)	(9)	(10)
MAPT w/ UBC	134.41	59.55	2.26	145.95	1.086	2.451	223.41	1.662	3.752
MAPT w/ Uniform				177.61	1.321	2.983	259.52	1.931	4.358
ANT w/ UBC	132.56	52.54	2.52	149.02	1.124	2.836	208.20	1.571	3.963
ANT w/ Uniform				188.99	1.426	3.597	253.92	1.916	4.833

The following conclusions result from the inelastic static analyses.

(1) For a given roof displacement level, the uniform load pattern produces larger base shear than the UBC-specified pattern. Since the uniform load pattern includes some contributions of the higher modes of vibration, this finding suggests that, for a given drift, the structural members, especially the columns, will experience larger shear forces when the higher modes of vibration are involved. Because shear forces can have an adverse effect on the ductility of structural members, it might be necessary to modify the transverse reinforcement details of members to improve their ductility performance when the structures are expected to be significantly influenced by the higher modes of vibration.

(2) The MAPT and ANT frames are adequately designed with regard to the strength requirements of the UBC code. The average overstrength factors against first yield under the UBC load pattern of the MAPT and ANT frames is 1.10 and that against failure is 1.62. The overstrength factor is defined as the yield or the ultimate load divided by the factored design seismic load. The yield and the ultimate load are the first yield load and the ultimate load obtained from the analyses.

(3) The MAPT and ANT frames can perhaps be qualified to be used in a more severe seismic zone such as the UBC zone 4, if the analytically calculated periods are taken into account and the reinforcement details are upgraded to meet the more severe requirements. As shown in Fig. 3-9, the design base shear varies roughly inversely with the fundamental period. Therefore, the design base shears computed using the analytically calculated periods (which are longer than the UBC periods) are smaller than that computed using the UBC periods. According to UBC provisions, the design seismic loads of the MAPT and ANT frames in UBC zone 4 are 1.56 times the design seismic loads of the frames in UBC zone 2A. Column (4) in Table 3-3 shows that the magnitudes of the seismic loads used in the designs of the MAPT and ANT frames are at least 2.25 times the required design seismic loads when the analytically calculated periods are used. In this regard, the MAPT and ANT frames meet the strength requirements of UBC zone 4.

3.3.3 Inelastic Dynamic Analyses

Table 3-4 summarizes the results of the inelastic dynamic analyses of the MAPT and ANT frames. The maximum story drifts of the frames under the three earthquake scenarios are plotted in Figs. 3-10 and 3-11. Comparisons between the maximum base shear versus roof displacement relationships obtained from the inelastic dynamic analyses and those from the inelastic static analyses are shown in Fig. 3-12.

Based on the above information, the following observations can be made. First, the MAPT and ANT frames responded elastically to the moderate and severe Nahanni-type earthquakes, and inelastically to the moderate and severe El Centro-type earthquakes. The magnitudes of the displacements and base shears of both frames under the Nahanni-type earthquakes were as low as 10% of those under the El Centro-type earthquakes. Second, the PGA magnitudes of the largest sustainable Nahanni-type earthquakes were at least 4.5 times the magnitudes of the largest sustainable El Centro-type earthquakes. Third, despite the large difference in the PGA magnitudes, the maximum responses (base shear, interstory drift, and roof displacement) of the MAPT and ANT frames under the largest sustainable earthquakes of both the Nahanni- and El Centro types were comparable. In addition, the maximum roof displacements under the largest sustainable earthquakes correlated well with the roof displacement magnitudes at the failure stage under static loads. Fourth, inelastic static analyses using the uniformly distributed load pattern provide better predictions, in general, of the maximum dynamic base shears and roof displacements of the MAPT and ANT frames under moderate and severe earthquakes than the UBC-specified pattern. Fifth, the static base shears were smaller than the dynamic base shears. Sixth, the PGA magnitudes of the largest earthquakes that could be sustained by the MAPT and ANT frames were much larger than the PGA magnitudes of the moderate earthquakes. The ratios between the PGA of the largest earthquakes and the moderate earthquakes are at least 20.7 times for the Nahanni-type and 3.86 times for the El Centro-type earthquakes. Finally, in the three earthquake scenarios, plastic hinges, if there were any, occurred only in the beams at the DHLs, and in the first story columns at their bases. Therefore, the MAPT and ANT frames always behaved in the strong column-weak beam fashion.

The first and second observations can be explained by reviewing the power spectral density analyses on both the Nahanni and El Centro ground acceleration records, Fig. 3-7. The figure shows that the Nahanni record has all of its dominant periods in the very low period range, roughly below 0.30 second. The El Centro record, on the other hand, has its dominant periods located in a higher period region of approximately 0.40 to 1.50 second. These findings indicate that the modes of vibration with smaller periods will govern the response behavior of structures subjected to Nahanni-type earthquakes, whereas the modes with larger periods will control the behavior of structures under El Centro-type earthquakes. For the MAPT and ANT frames, these findings mean that the fourth and higher modes will govern the response under Nahanni-type earthquakes, and second to fourth modes will control under El Centro-type earthquakes. Due to its long natural period, the first mode of vibration of both MAPT and ANT frames will not respond actively to the excitations from either earthquake type.

Inertia forces along the height of structures tend to accumulate when the response behavior of structures is controlled by the lower modes of vibration. They also are likely to cancel each other under the higher modes. As a result, the responses of the MAPT and ANT frames under the El Centro-type earthquakes, which have a dominant period range of 0.40 to 1.50 second, can be much larger than the responses under the Nahanni-type earthquakes that have comparable PGA magnitudes. It will take a Nahanni-type earthquake with much larger PGA magnitude than that of an El Centro-type to bring the MAPT and ANT frames to their maximum capacities.

With regard to the third observation, strong column-weak beam mechanisms formed in the MAPT and ANT frames under both the largest sustainable Nahanni- and El Centro-type earthquakes.

Table 3-4 Summary of Results of Inelastic Dynamic Analyses

Frame	Scenario	EQ. Record ID. (x Scale Factor)	PGA	Max. Base Shear	Max. Interstory Drift*		Max. Roof Displacement	Ductility Demand- to-Supply Ratio**		Plastic Hinge Locations (B = Beam, C = Column)
				(kip)	(in.)	Floor	(in.)	Max.	Floor	
(1)	(2)	(3)	(4)	(5)	(6)	(7)	(8)	(9)	(10)	(11)
MAPT	Moderate EQ.	Nahanni (x 1.00)	0.148g	24.76	0.16	7	0.79	-	-	-
		El-Centro (x0.50)	0.174g	234.98	1.31	7	6.70	0.24	2	B: 1st to 7th fls.
	Severe EQ.	Nahanni (x 2.00)	0.296g	57.09	0.32	7	1.58	-	-	-
		El-Centro (x1.00)	0.348g	280.87	1.61	8	8.32	0.38	2, 3	B: all fls.; C: all 1st fl. int. bases
	Largest EQ.	Nahanni (x 24.06)	3.561g	351.42	3.10	3	13.60	1.00	3	B: all fls.; C: all 1st fl. bases
		El-Centro (x 1.93)	0.670g	341.99	2.99	4	14.56	1.00	3	B: all fls.; C: all 1st fl. bases
ANT	Moderate EQ.	Nahanni (x 1.00)	0.148g	27.35	0.19	3, 4	1.04	-	-	-
		El-Centro (x0.50)	0.174g	158.99	1.51	7	7.72	0.35	7	B: 7th fl.
	Severe EQ.	Nahanni (x 2.00)	0.296g	54.67	0.39	3, 4	2.07	-	-	-
		El-Centro (x1.00)	0.348g	274.65	2.13	5, 6	9.85	0.49	7	B: all fls.; C: all 1st fl. int. bases
	Largest EQ.	Nahanni (x 20.71)	3.065g	342.46	3.28	4	16.06	1.00	7	B: all fls.; C: all 1st fl. bases
		El-Centro (x 1.97)	0.685g	338.35	3.51	4	17.60	1.00	3	B: all fls.; C: all 1st fl. bases

Remarks: * Interstory drift is defined as the difference between the lateral displacement of two consecutive floors. The floor level listed in the table is the upper floor.

** Ductility demand-to-supply is the ratio between the rotational ductility demand and the rotational ductility capacity of a plastic hinge. The maximum ratios are not listed when the frames remained elastic and no plastic hinge occurred. When the frames responded inelastically to the earthquakes, the maximum demand-to-supply ratios are listed along with the floor at which they occur. All maximum ratios were found at the beam plastic hinges at the DHLs. Plastic hinges were detected only at the DHLs and at the bases of first story columns.

With the same failure mechanism, the same prescribed maximum rotational capacities, and the same type of loading (dynamic loads), the magnitudes of the base shear and the displacement responses of the frames should be comparable. A partial strong column-weak beam mechanism also occurred at the ultimate stage under static loading. Because dynamic and static loads are different in nature, the maximum base shear magnitudes under dynamic and static loads might or might not be similar. However, with the same failure mechanism and the same prescribed rotational capacities, the maximum displacement responses obtained from the dynamic and static analyses must still be reasonably close.

With regard to the fourth observation, the UBC load pattern represents the case when the first mode of vibration governs the response behavior, and the uniform load pattern includes some higher mode contributions. As discussed earlier, the higher modes of vibration control the responses of the MAPT and ANT frames under both the Nahanni- and El Centro-type earthquakes. The inelastic analyses based on the uniform load pattern, therefore, provide better predictions to the dynamic responses of both frames than the results based on the UBC load pattern.

The difference between the magnitudes of base shear computed using the inelastic static and inelastic dynamic analyses, reported in the fifth observation, is believed to result from the participation of the higher modes of vibration. As mentioned earlier, the inertia forces induced by the higher modes of vibration tend to cancel each other. The centroids of the total inertia forces on the MAPT and ANT frames, which are controlled by the higher modes of vibration, are therefore likely to be located closer to the ground level than the centroids of the UBC and the uniform load patterns. Because the moment arms from the centroids of the forces to the supports of the structures are shorter, larger inertia forces are needed to yield the structures and to bring them to their ultimate stage. As a result, the MAPT and ANT frames had larger ultimate loads for dynamic analyses.

The sixth observation, that the MAPT and ANT frames have the ability to undergo an earthquake with a PGA much larger than the design PGA magnitude, indicates that both frames have very significant reserve seismic capacities. The MAPT and ANT frames, and thus the prototype structure, can therefore be utilized in a more active seismic region, such as UBC zone 4. To qualify for use in zone 4, however, the transverse reinforcement details of the frames will have to be modified to satisfy the minimum requirements of the UBC provisions.

Based on the final observation, it is concluded that strong column-weak beam behavior can be enforced successfully using the proposed design methodologies.

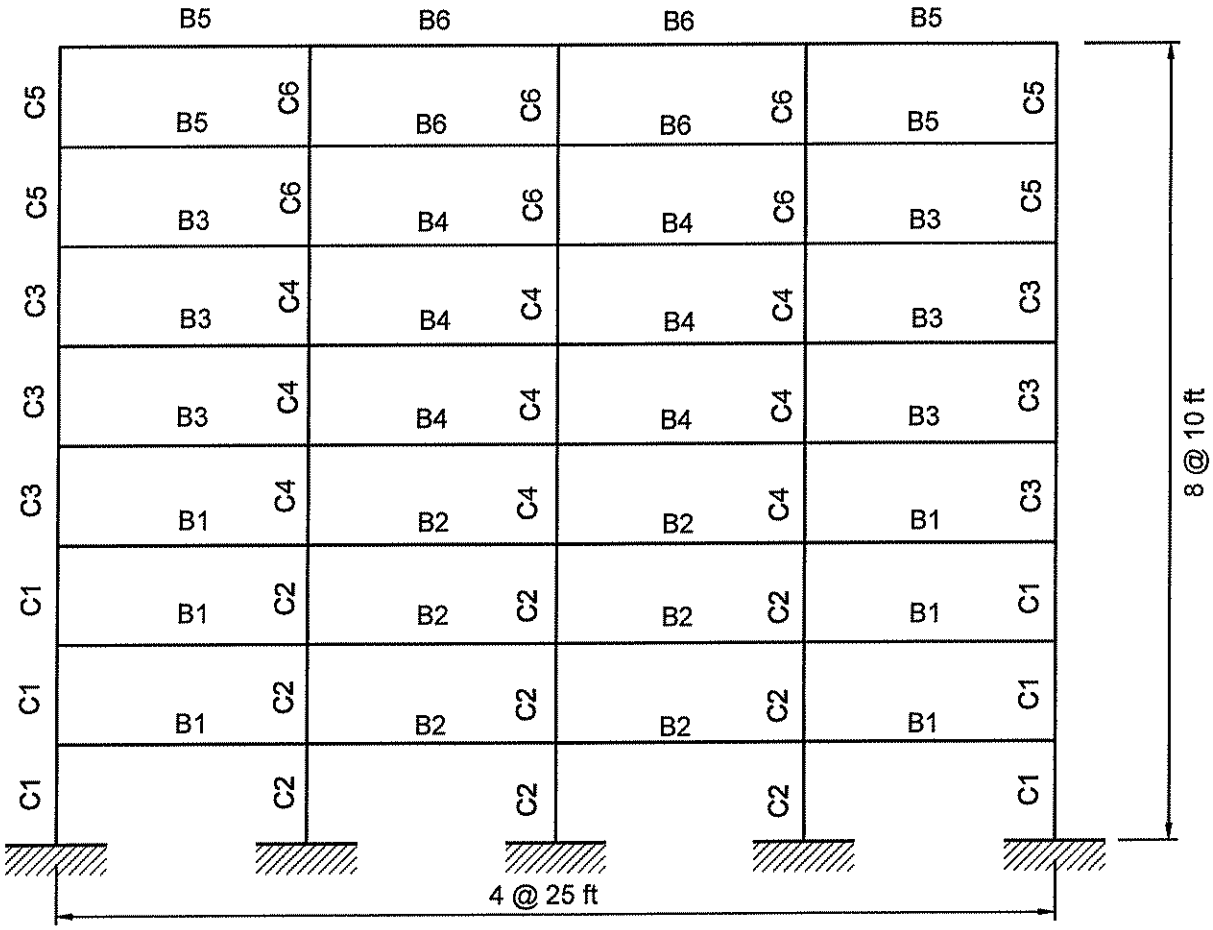

Figure 3-1 Elevation of MAPT and ANT Frames with Member Identification

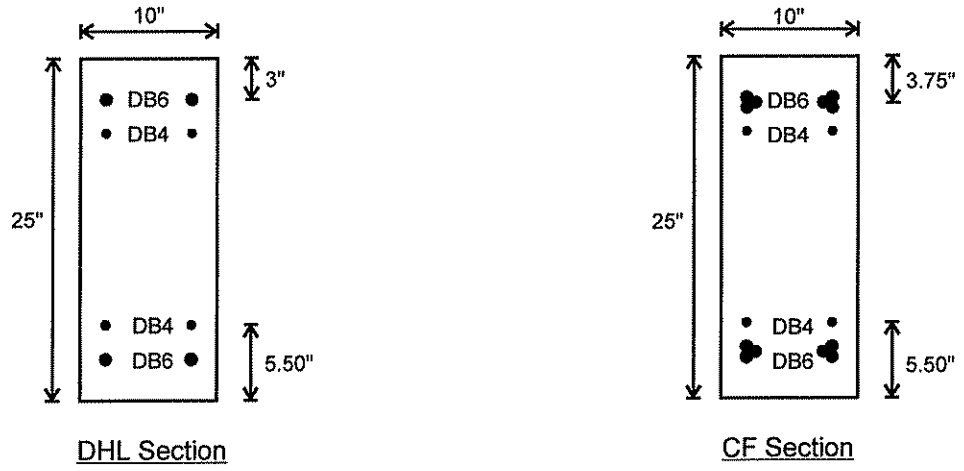

Beams B1 to B4

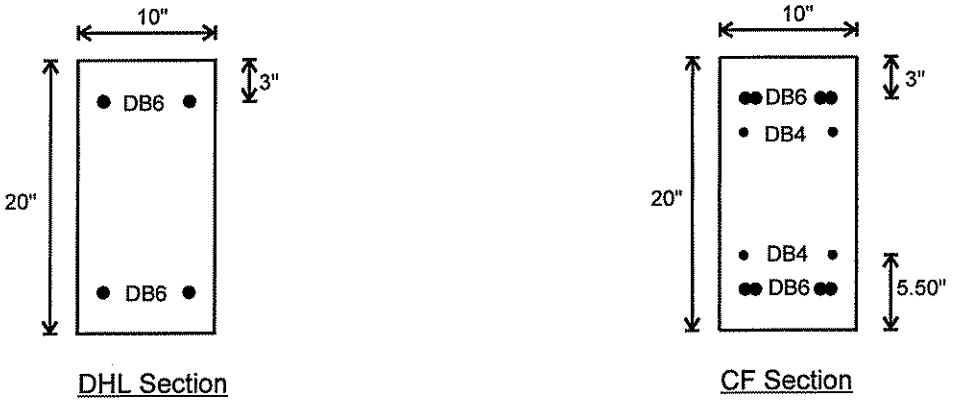

Beams B5 and B6

Figure 3-2 Cross-Sections of Beam Sections of MAPT Frame

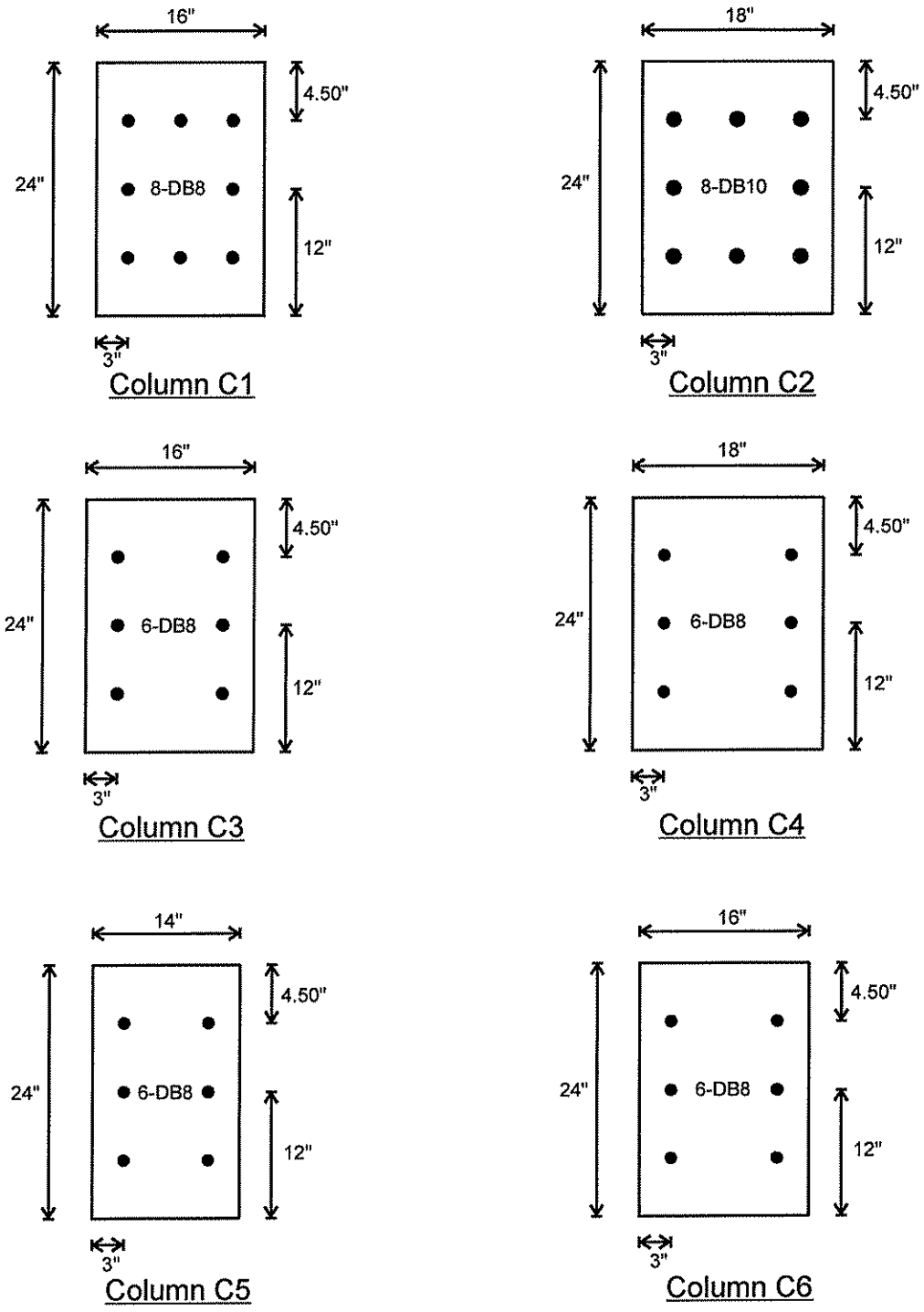

Figure 3-3 Cross-Sections of Column Sections of MAPT Frame

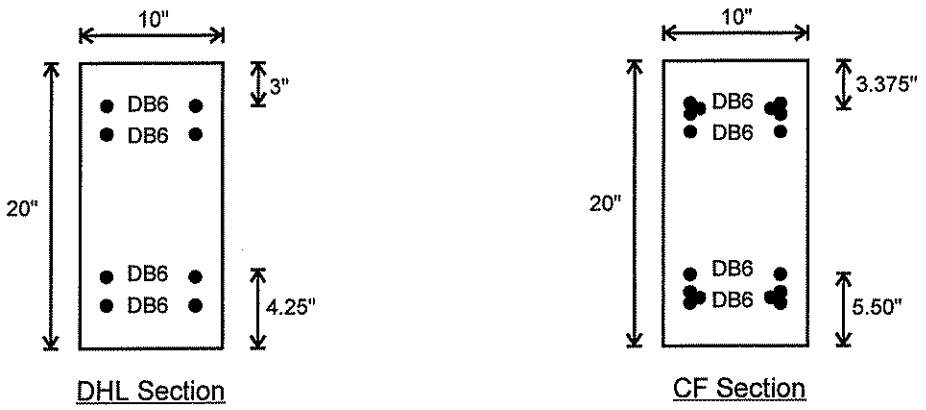

Beams B1 and B2

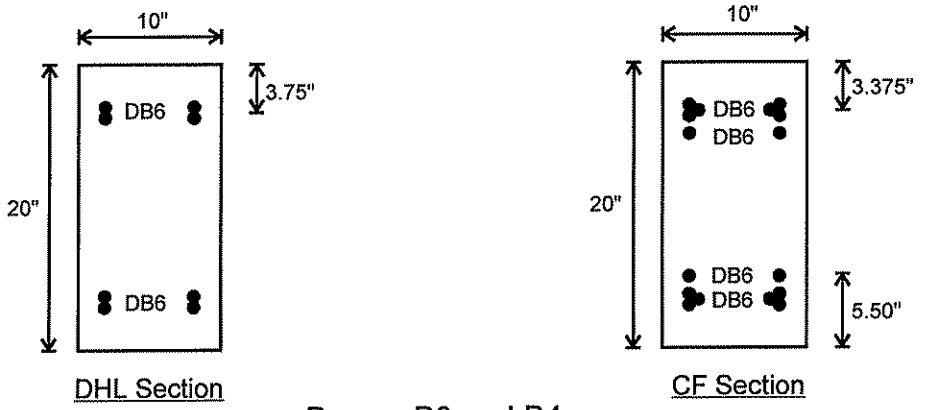

Beams B3 and B4

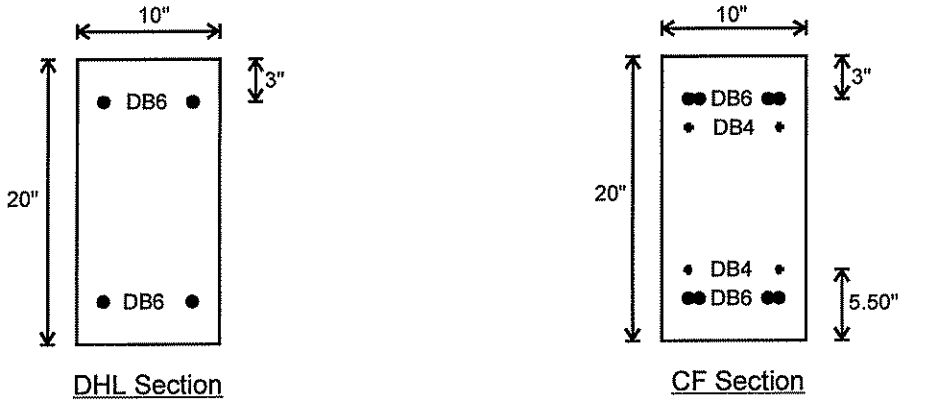

Beams B5 and B6

Figure 3-4 Cross-Sections of Beam Sections of ANT Frame

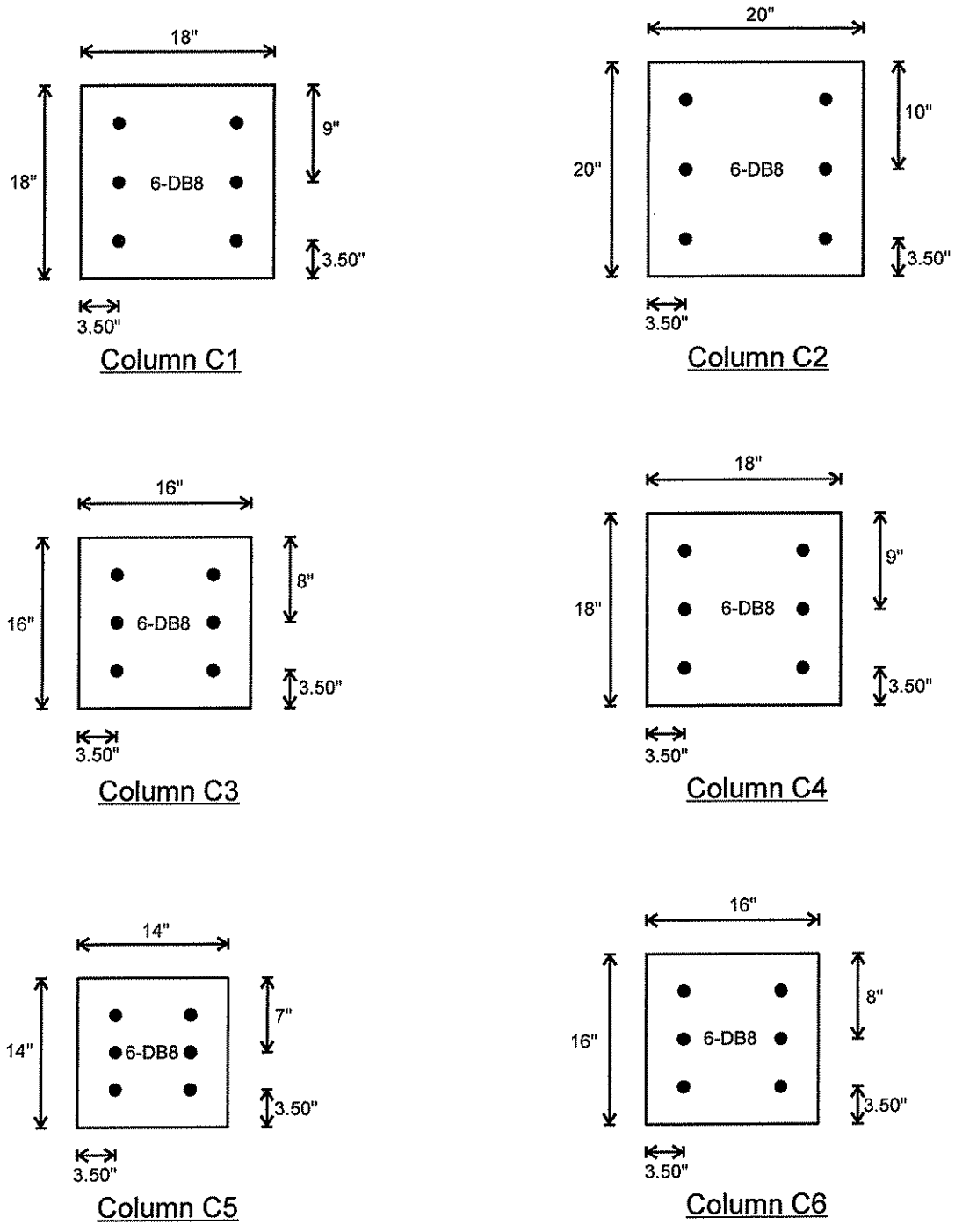

Figure 3-5 Cross-Sections of Column Sections of ANT Frame

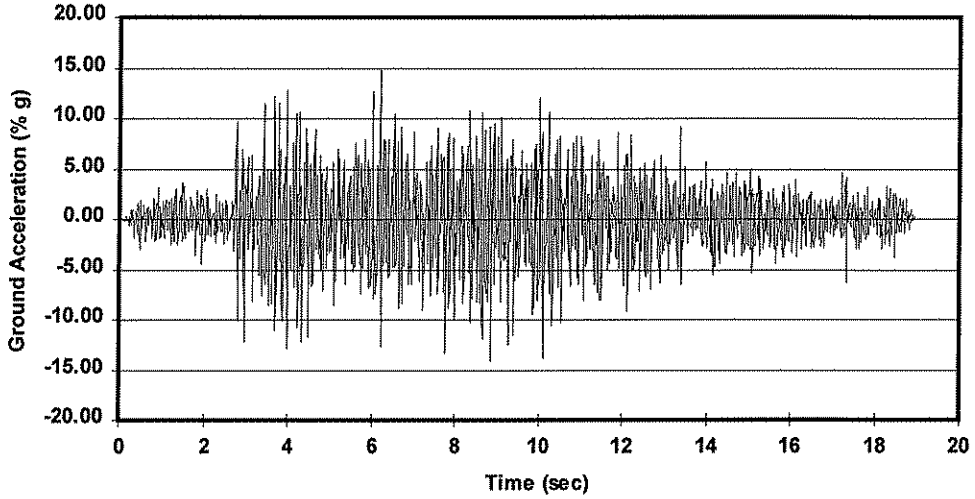

(a) Nahanni Ground Acceleration Record

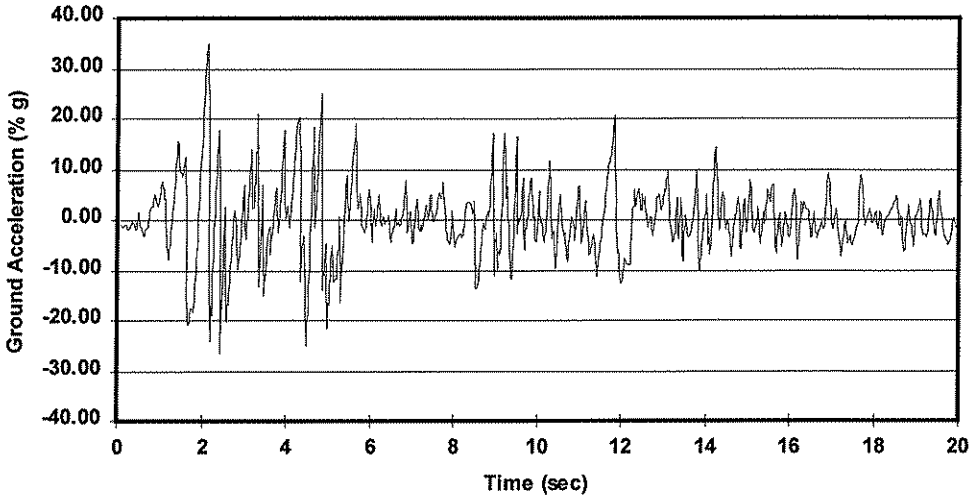

(b) El Centro Ground Acceleration Record

Figure 3-6 Ground Acceleration Records Utilized in Inelastic Dynamic Analyses

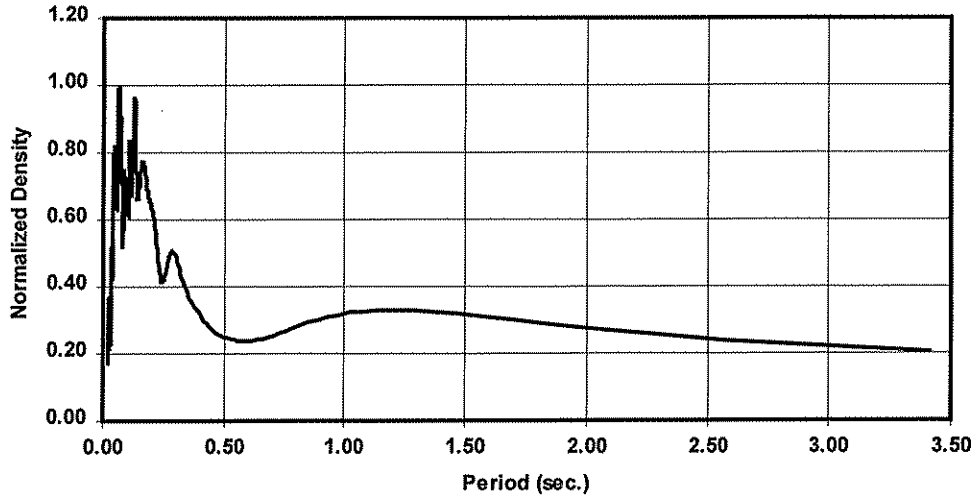

(a) Nahanni Record

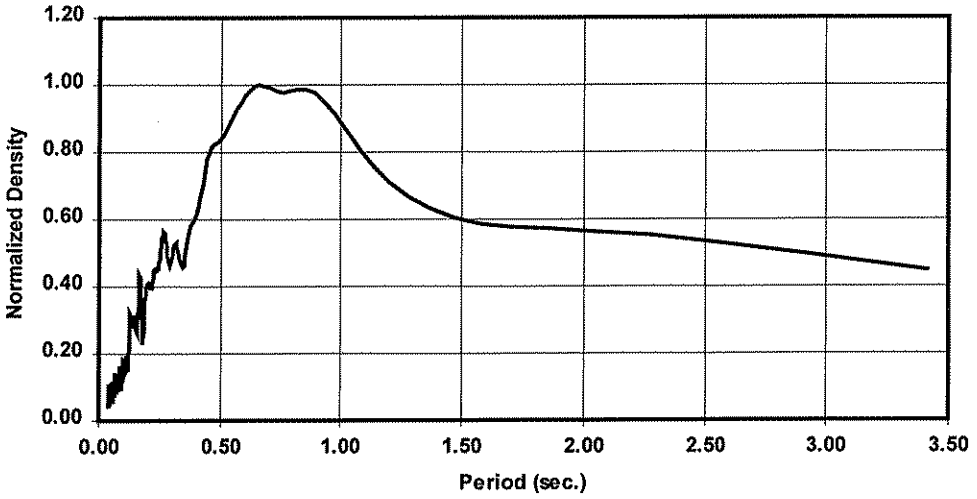

(b) El Centro Record

Figure 3-7 Normalized Power Spectral Density of Nahanni and El Centro Ground Acceleration Records

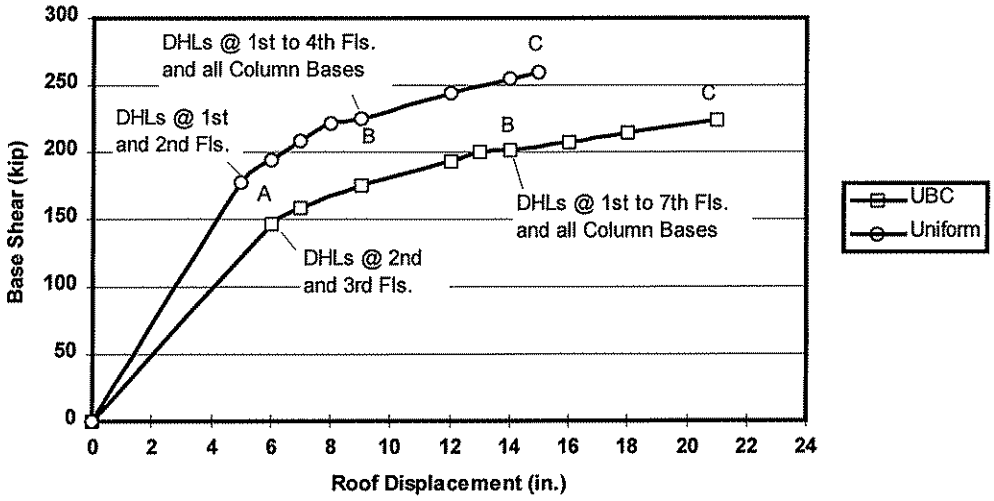

(a) MAPT Frame

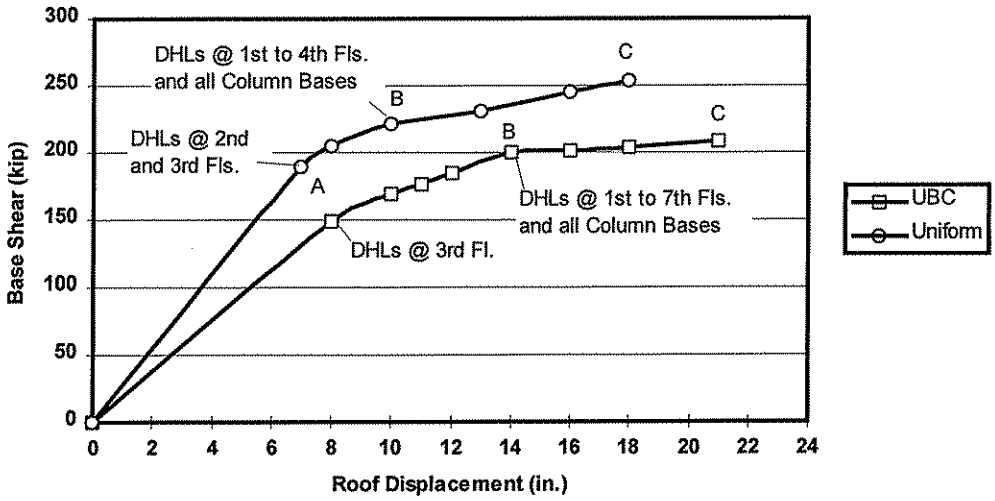

(b) ANT Frame

Figure 3-8 Static Base Shear *vs.* Roof Displacement Relationship for Frames

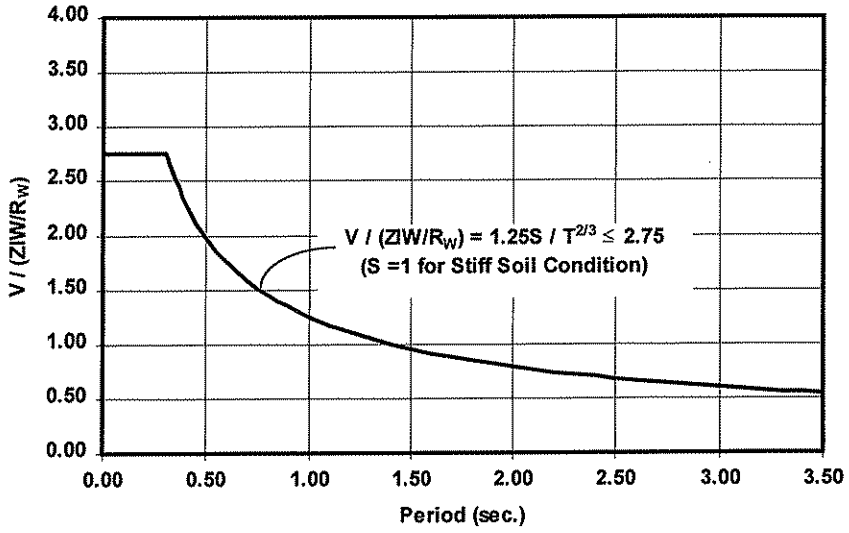

Figure 3-9 Relationship between Design Base Shear and Period of Structures Located on a Stiff Soil Site

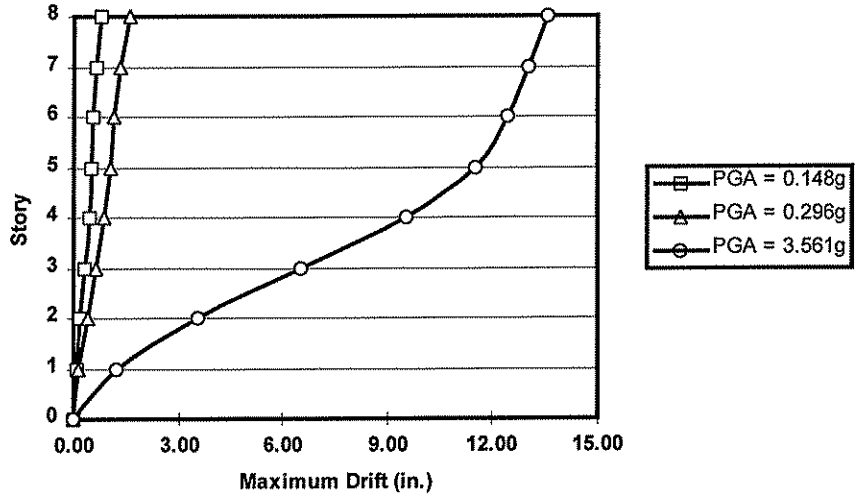

(a) Under Nahanni Record

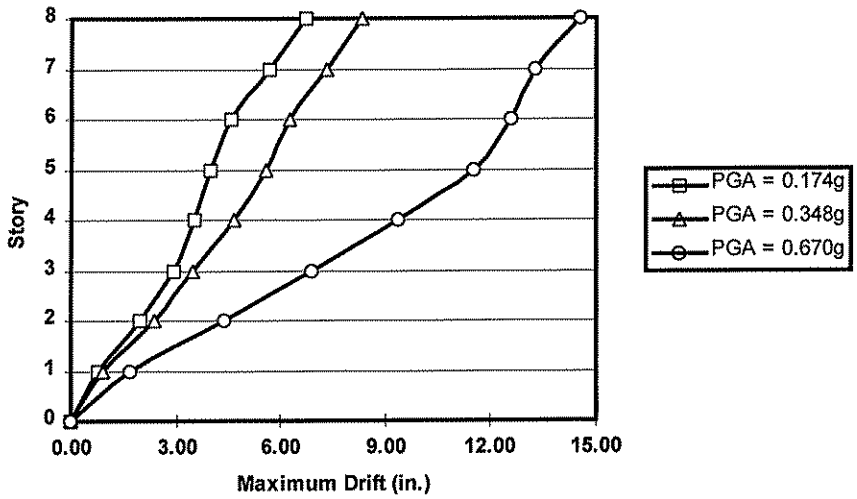

(b) Under El Centro Record

Figure 3-10 Maximum Story Drifts of MAPT Frame under Three Earthquake Scenarios

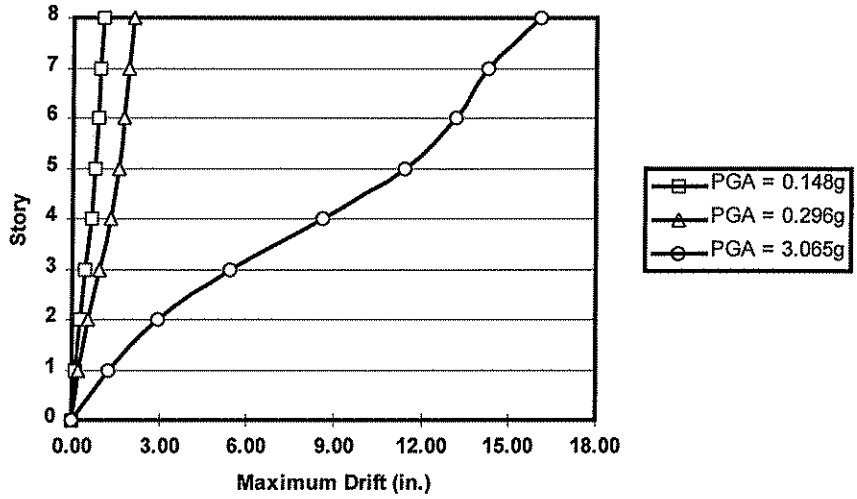

(a) Under Nahanni Record

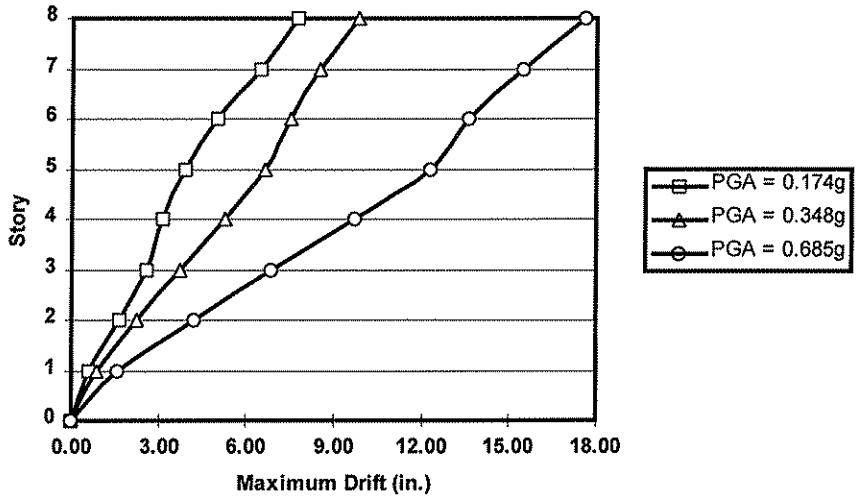

(b) Under El Centro Record

Figure 3-11 Maximum Story Drifts of ANT Frame under Three Earthquake Scenarios

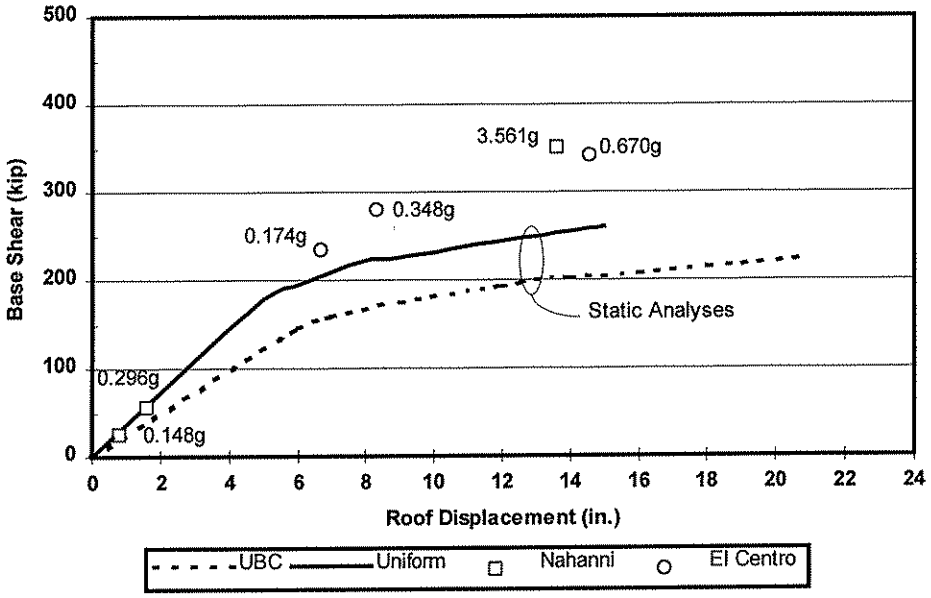

(a) MAPT Frame

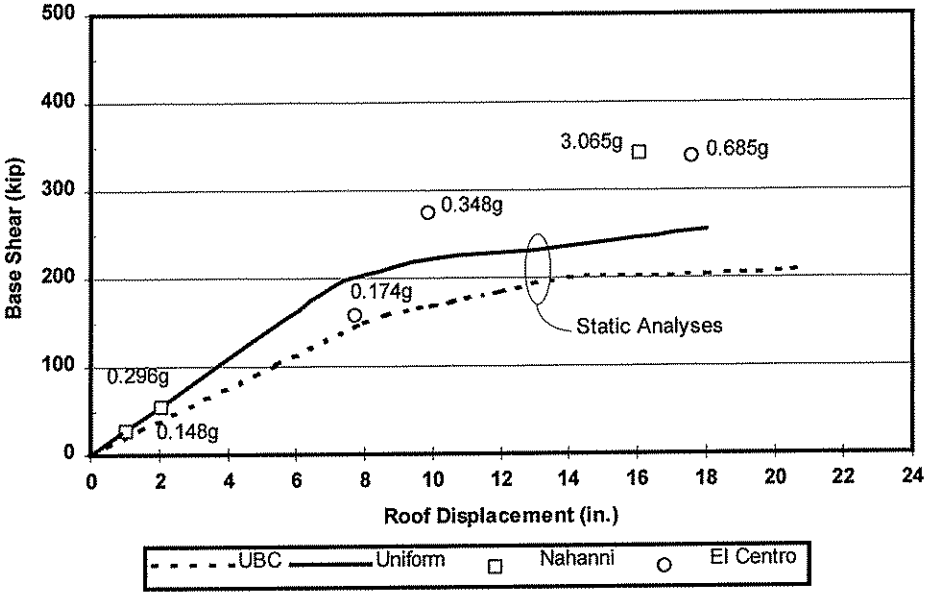

(b) ANT Frame

Figure 3-12 Comparison of Static and Dynamic Base Shear *vs.* Roof Displacement

4.0 SUMMARY

This report has focused on design examples for ATLSS Precast Concrete (APC) Systems, and on seismic analyses of frames incorporating APC systems.

Design examples for regular and exterior assemblies of both MAPT- and ANT-type frame systems were developed using earthquake load combinations for a moderate seismic zone. Concrete strengths were either 4000 psi or 6000 psi. The design methodologies retain the philosophy of a strong column - weak beam behavior for seismic resistant building frames. The methodologies are strength-based to be independent of a specific seismic zone. Beams and columns should be designed using the provisions of the ACI 318 code, with the designated hinging locations (DHLs) located away from the column faces. The methodology for designing APC connections is based on a 2-D strut-and-tie model, which includes the connection and portions of the beams and columns bounded by their points of contraflexure. Connection reinforcement is proportioned to resist all splitting tensile forces. Appropriate consideration is given to constructability.

To evaluate the seismic adequacy of the design methodologies, both inelastic static and inelastic dynamic seismic analyses were performed for both MAPT- and ANT-type frames, using the software DRAIN-2DX. The inelastic static analyses of the frames were carried out using two seismic-equivalent lateral load patterns: The UBC pattern where the first mode of vibration governs the behavior and a uniformly distributed load pattern where the higher modes of vibration have a more significant effect. For the inelastic dynamic analyses, the frames were subjected to ground acceleration records from the Nahanni and the El Centro earthquakes. The PGA magnitude of both records were scaled as necessary to represent three earthquake scenarios; moderate, severe, and the largest sustainable. The ratios between the PGA magnitudes of the largest sustainable earthquakes and of the moderate earthquakes were at least 20.7 and 3.86, with the Nahanni- and the El Centro-type records, respectively.

The natural periods of the frames were computed prior to the analyses and showed that the natural periods of both MAPT and ANT frames are sensitive to the orientation of the precast floor slabs. The natural period of the APC frames (and probably any frame structure utilizing precast floor slabs) can be much longer when the precast floor slabs are oriented parallel, instead of perpendicular, to the frames. This suggests that analytically calculated, rather than code-prescribed, periods should be used in seismic-resistant structural design involving precast floor slabs.

In the inelastic static analyses, the uniformly distributed load pattern produced larger base shears than the UBC-specified load pattern, for a given magnitude of roof displacement. Thus, structural members, especially columns, are likely to carry larger shear forces when the structural behavior is significantly affected by higher modes of vibration. However, the analyses showed that the MAPT and ANT frames were adequately designed to meet the strength requirement of the UBC code. When the code-prescribed periods were used, the average overstrength factors with respect to the first yield and the ultimate stage of both frames were 1.10 and 1.62, respectively. Moreover, if the analytically computed periods of the frames were considered and the reinforcement details of the frames were upgraded to meet the requirements of the UBC provisions, the MAPT and ANT frames could be qualified for use in a severe seismic zone such as the UBC zone 4.

The inelastic dynamic analyses indicated that the responses of the MAPT and ANT frames to the Nahanni- and El Centro-type earthquakes were governed by the higher modes of vibration, but the frames had sufficient strength and ductility to sustain large earthquakes of both types before failure.

Both the inelastic dynamic and the inelastic static analyses demonstrated that higher modes of vibration had significant effects on the MAPT and ANT frames. But the results of both analyses also suggest that both types of frames can be utilized, with proper detailing, in UBC zone 4. In addition, it was found that both frames exhibit strong column-weak beam behavior in all the earthquake scenarios. Therefore, it is concluded that the proposed design methodologies are appropriate.

REFERENCES

[1] J. Kanatharana, L-W Lu, and B.V. Viscomi
ATLSS Precast Concrete Systems: Review of Existing Systems and New Conceptual Developments
ATLSS Report No. 96-10-01, July 1996

[2] J. Kanatharana, L-W Lu, and B.V. Viscomi,
ATLSS Precast Concrete Systems: Design Methodology and Performance Evaluation
ATLSS Report No. 96-10-02, December 1996

[3] American Concrete Institute (ACI)
Building Code Requirements for Reinforced Concrete (ACI 318), 1989 Edition
ACI, Detroit, MI, 1989

[4] B. Abdel-Fattah and J.K. Wight
Study of Moving Beam Plastic Hinging Zones for Earthquake-Resistant Design of R/C Buildings,
ACI Structural Journal, Vol. 84, No. 1, Jan-Feb 1987, pp 31-39

[5] M.S. El-Haddad and J.K. Wight
Relocating Beam Plastic Hinging Zones for Earthquake-Resistant Design of Reinforced Concrete Design
ACI Structural Journal, Vol. 85, No. 2, Mar-Apr 1988, pp 123-133

[6] J. Schlaich, K. Schafer, and M. Jennewein
Toward a Consistent Design of Structural Concrete
PCI Journal, Vol. 32, No. 3, May-June 1987, pp 74-150

[7] V. Prakash, G.H. Powell, and S. Campbell
DRAIN-2DX Base Program Description and User Guide, Version 1.10
Report No. UCB/SEMM-93/17, Dept. of Civil Engineering, University of California at Berkeley, November 1993

[8] M. Wakabayashi
Design of Earthquake-Resistant Buildings
McGraw-Hill Book Company, New York, NY, 1986

[9] R.W. Clough and J. Penzien
Dynamics of Structures, 2nd Edition
McGraw-Hill Book Company, New York, NY, 1993

[10] International Conference of Building Officials (ICBO)
Uniform Building Code, 1988 Edition
ICBO, Whittier, CA, 1988

[11] S. Wu
Seismic Analysis and Retrofit of Non-Ductile Reinforced Concrete Frame Buildings
Dissertation presented in partial fulfillment of the requirements for the Degree of Doctor of Philosophy in Civil Engineering, Lehigh University, Bethlehem, PA, September 1995